Supporting information

Cu(II) templated formation of [n]Pseudorotaxanes (n= 2,3,4) using a tris-amino ether macrocyclic wheel and multidentate axles

Somnath Bej, Mandira Nandi, Tamal Kanti Ghosh and Pradyut Ghosh*

School of Chemical Sciences, Indian Association for the Cultivation of Science, 2A & 2B Raja S. C. Mullick Road, Kolkata 700032, India. E-mail: icpg@iacs.res.in

List of contents

- X-ray crystallographic data details……..**S3**
- Calculation of Association Constants…….…..**S3**
- Synthesis route of **NaphMC (Scheme 1S)**……..**S4**
- Synthetic route of **Phen-Acid (Scheme 2S)**……**S4**
- Characterization of compound **A (Figure 1S- Figure 3S)**……**S5-S6**
- Characterization of **L2 (Figure 4S- Figure 6S)**…… **S6-S7**
- Characterization of compound **B (Figure 7S- Figure 9S)**……..…..**S8-S9**
- Characterization of **L3 (Figure 10S- Figure 12S)**……. **S9-S10**
- Synthetic route of **NaphMC-Cu(II)** complex **(Scheme 3S)**…….....…**S11**
- ESI-MS spectra of **[2], [3], [4]**pseudorotaxanes (**Figure 13S- Figure 15S).... .S11-S12**
- Equivalent plots of **[2], [3], [4]**pseudorotaxanes **(Figure 16S- Figure 18S)….S13-S14**
- Molar ratio plots of **[2], [3], [4]**pseudorotaxanes **(Figure 19S- Figure 21S)…S14-S15**
- Characteristic UV/Vis and emission spectra of **[**n**]**Pseudorotaxanes **(Figure 22S)..S16**
- Nonlinear curve fitting plot for the formation of **[2]**pseudorotaxane (**Figure 23S)..S16**
- Nonlinear curve fitting plot for the formation of **[3]**pseudorotaxane (**Figure 24S)..S17**
- Crystallographic details **(Table 1S** and **Figure 25S- Figure27S)**…….**S17-S19**
- EPR spectra of **[2], [3], [4]**pseudorotaxanes **(Figure 28S- Figure 30S) ……..…..S20**
- Synthetic route of **L4 (Scheme 4S)**….……..…...**S21**
- Characterization of compound **C** (**Figure 31S- Figure 32S)**……..….**S21-S22**
- Characterization of **L4** (**Figure 33S- Figure 35S)**……..……...**S22-S23**

- ESI-MS spectrum of **L4** axle based threaded molecule **(Figure 36S)…….....S24**
- UV/Vis titration profile between **L4** with **NaphMC-Cu**(II) **(Figure 37S)……..S24**
- Molar ratio plot of titration between **L4** with **NaphMC-Cu**(II) **(Figure 38S)……S25**
- IR spectra of **[2], [3]** and **[4]**pseudorotaxanes **(Figure 39S- Figure 41S)…….S25-S26**
- Synthetic route of **NaphMC-Ni**(II) complex **(Scheme 5S)……...……S27**
- ESI-MS spectrum of **NaphMC-Ni**(II) complex (**Figure 42S**)**……..S27**
- Synthetic route of Ni(II) based Pseudorotaxane **(Scheme 6S)…….S28**
- ESI-MS spectra of Ni(II) based pseudorotaxane **(Figure 43S- Figure 45S)…S28-S29**
- UV/Vis titration of Ni(II) based pseudorotaxanes **(Figure 46S- Figure 48S)...S30-S31**
- Molar ratio of Ni(II) based pseudorotaxanes **(Figure 49S- Figure 51S)……..S31-S32**
- Characteristic UV/Vis spectra of Ni(II) based pseudorotaxanes (**Figure 52S**)**…….S33**
- References**……..…S34**

X-ray crystallographic data details:

All the X-ray crystallographic details of **{[2]CuPR}$^{2+}$** were given in Table 1S. Single green block-shaped crystals of **[2]pseudorotaxane{[2]CuPR}$^{2+}$** were obtained upon slow evaporation of a solution of **[2]CuPR$(ClO_4)_2$** and excess NaOTf in CH_3CN. A suitable crystal 0.06×0.03×0.02 mm^3 was selected and mounted on a suitable support on an Bruker APEX-II CCD diffractometer using the SAINT/ SMART APEX II software. [1, 2] The crystal was kept at a steady T = 127 K during data collection. The structure was solved with the ShelXT 2014/5[3] structure solution program using suitable methods and by using Olex2[4] as the graphical interface. The model was refined with version 2018/3 of ShelXL[5] using Least Squares minimisation. SADABS[6] was applied for empirical absorption corrections. PLATON[7] and MERCURY 3.7[8] were used to generate graphical pictures of **{[2]CuPR}$^{2+}$**.

Calculation of Association Constants:

The association constants were calculated from UV/Vis titration experiments by plotting the absorbance changes (ΔA) at a fixed λ value against the guest concentration by using nonlinear fitting of the curves. Equation 1 is used for 1: 1 (host: guest) binding model[9]

$$\Delta A = \left(\frac{A}{2*H}\right) * \left\{\left(G_0 + H_0 + \frac{1}{K}\right) - \sqrt[2]{\left(G_0 + H_0 + \frac{1}{K}\right)^2 + 4G_0H_0}\right\} \ldots (1)$$

Where, A= absorbance intensity value upon each addition of the guest, change in absorption intensity $\Delta A = (A - A_0)$, $[H]_0$ = initial concentration of the host, $[G]_0$ = initial concentration of the guest and K is the association constants.

Similarly, equations 2 is used for non-linear curve fitting of 1:2 (host: guest) binding model.[10]

$$\Delta A = \frac{A_{\Delta HG1}K_1[H]_0[G] + A_{\Delta HG2}K_1K_2[H]_0[G]^2}{1 + K_1[G] + K_1K_2[G]^2} \quad \ldots\ldots\ldots\ldots\ldots\ldots\ldots\ldots (2)$$

Where, K_1 and K_2 are the stepwise association constants.

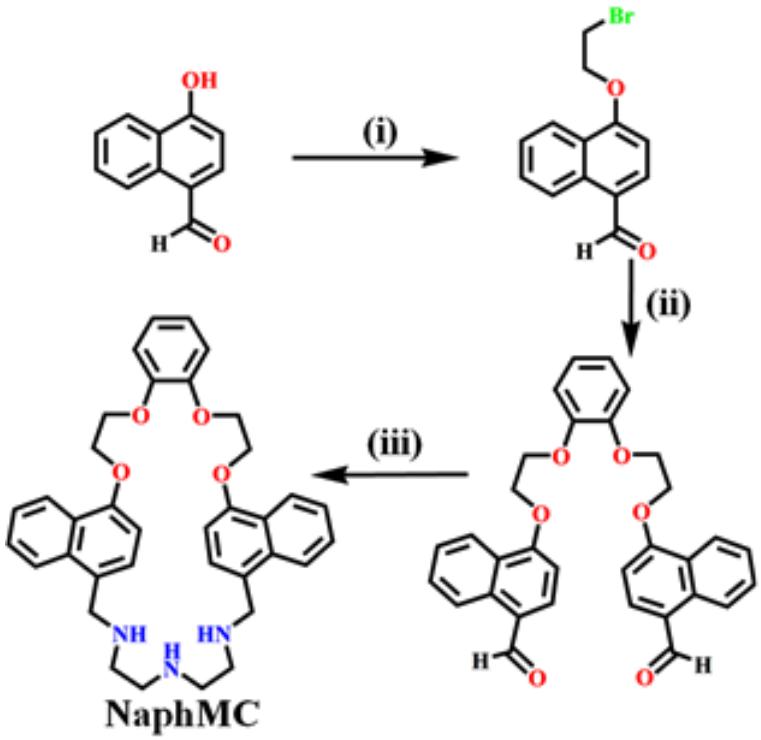

Scheme 1S. Synthesis route of **NaphMC**[11]: (i) 1,2-dibromoethane, K_2CO_3, CH_3CN, reflux; (ii) 1,2-dihydroxybenzene, K_2CO_3, CH_3CN, reflux; (iii) diethylenetriamine, CH_2Cl_2-CH_3OH, RT, 15h, $NaBH_4$.

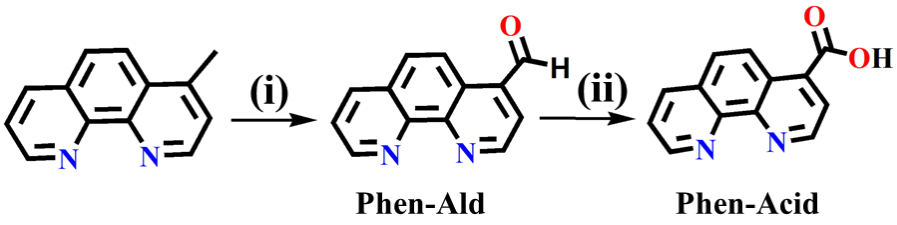

Scheme 2S. Synthetic route of **Phen-Acid**[12] :(i) SeO_2, dioxane, reflux;(ii) Conc. HNO_3, reflux.

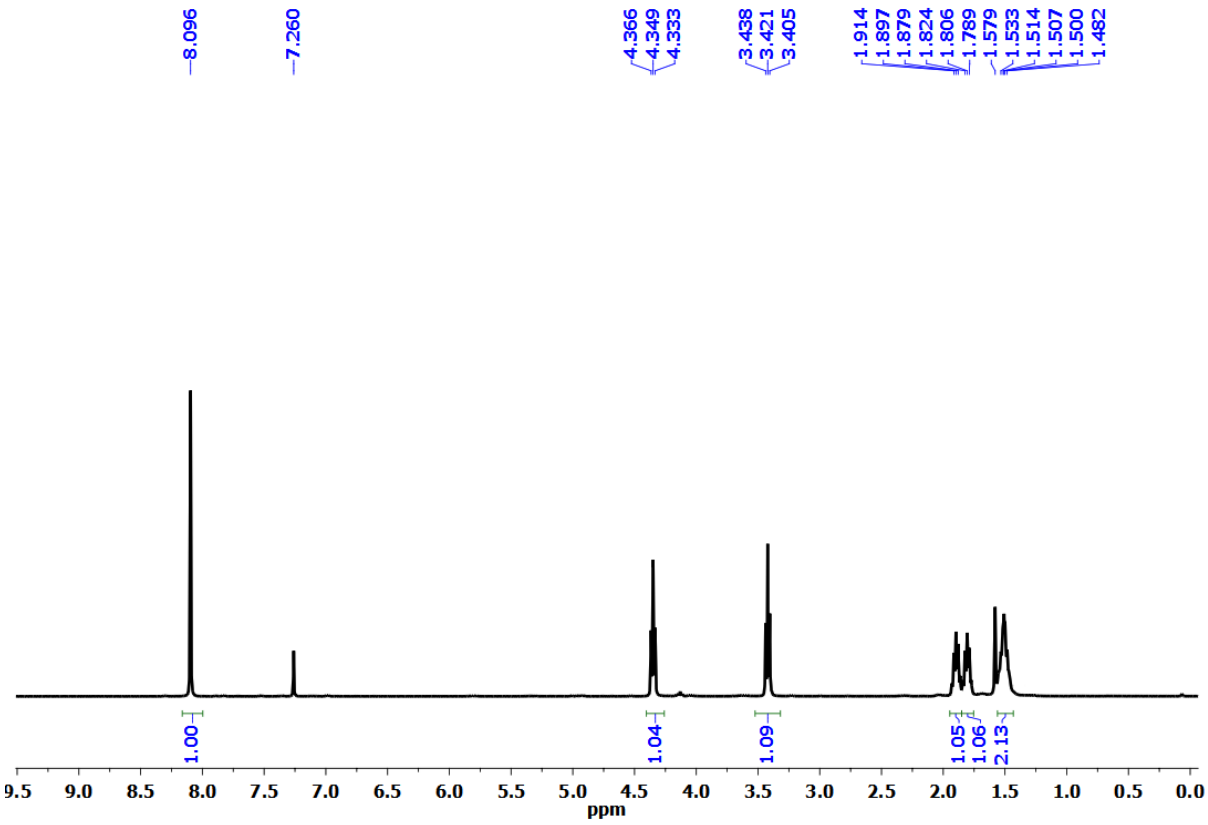

Figure 1S. ^{1}H-NMR spectrum of compound **A** in $CDCl_3$ in 400 MHz at 298K.

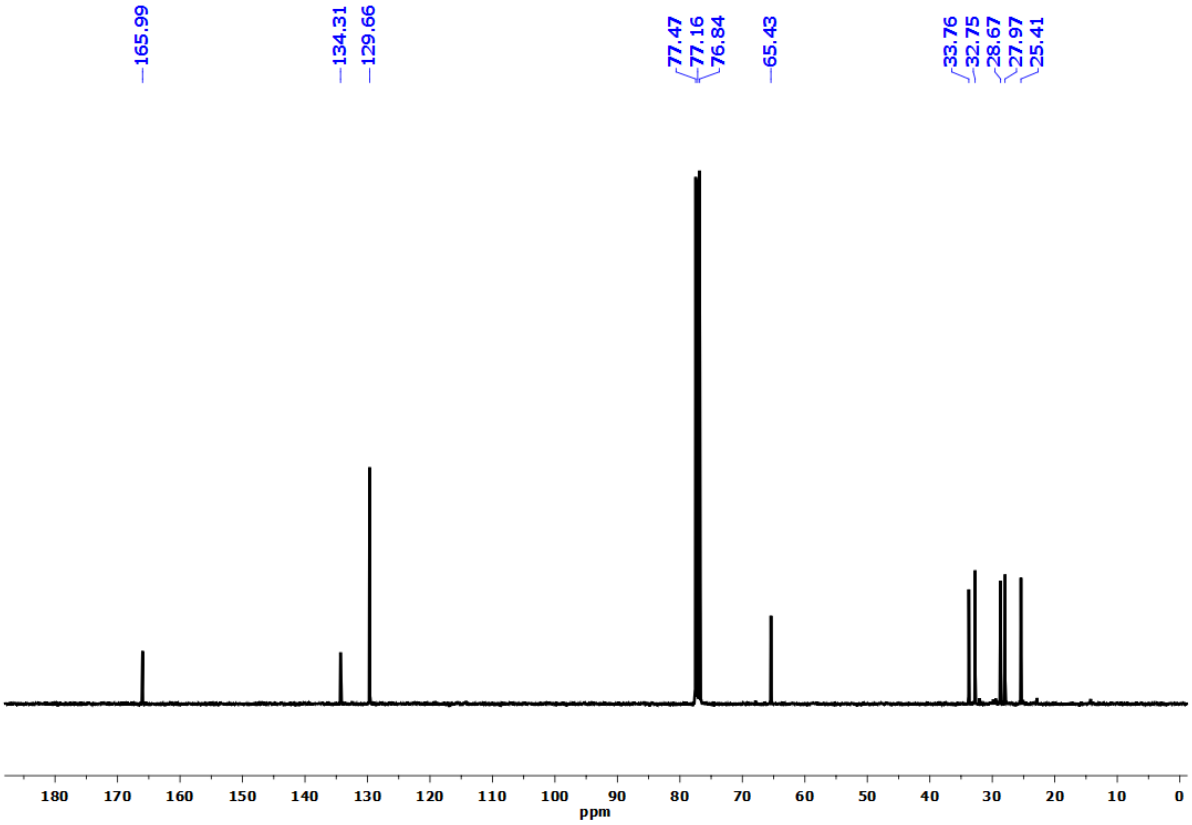

Figure 2S. ^{13}C-NMR spectrum of compound **A** in $CDCl_3$ in 100 MHz at 298K.

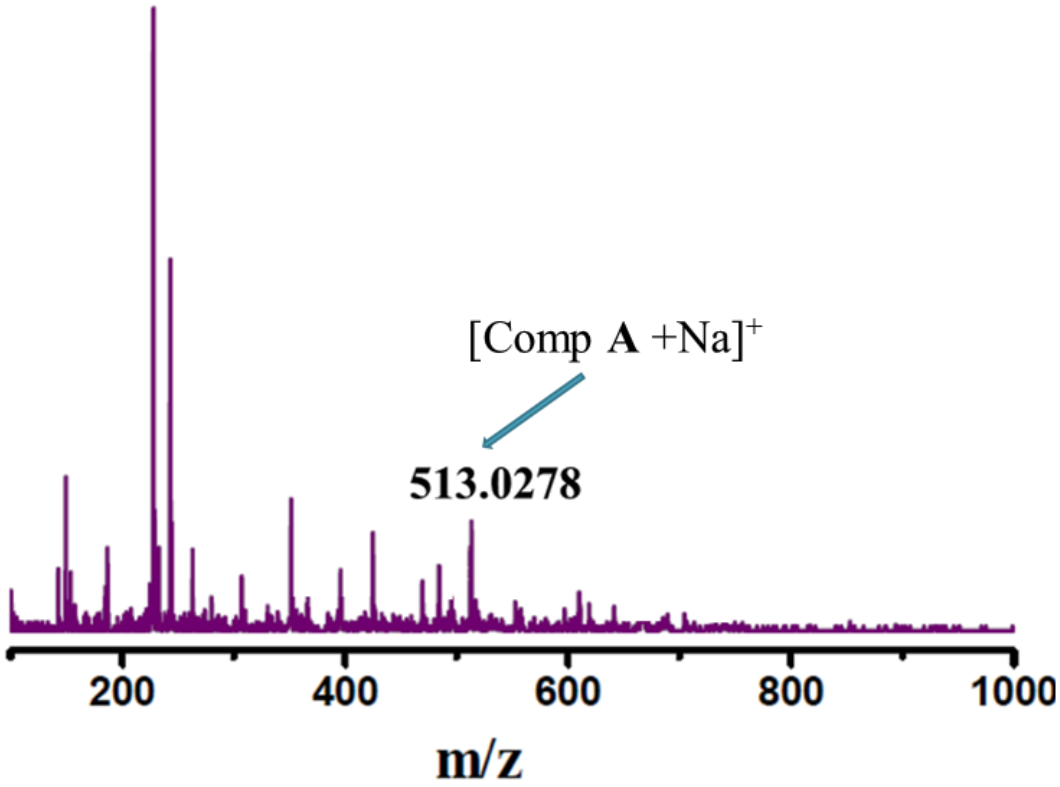

Figure 3S. ESI-MS(+ve) spectrum of compound **A** at 298K.

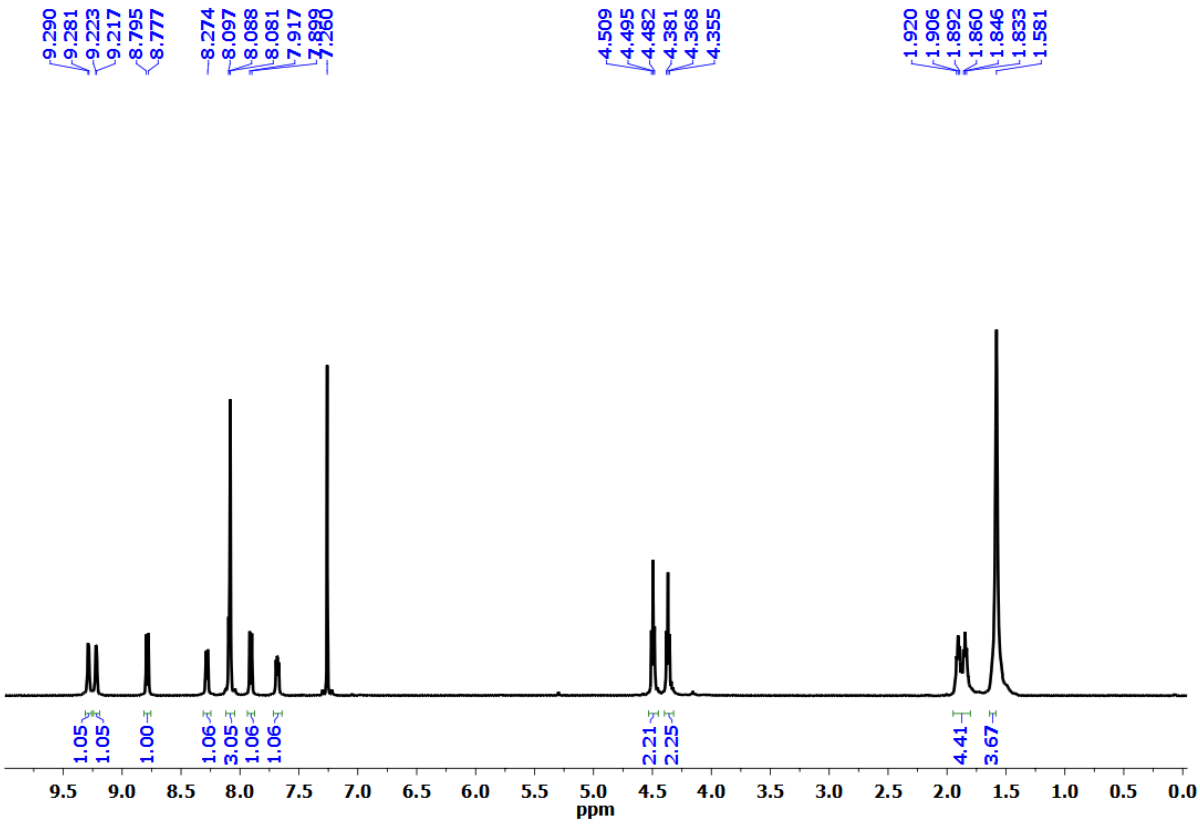

Figure 4S. ^{1}H-NMR spectrum of **L2** in $CDCl_3$ in 500 MHz at 298K.

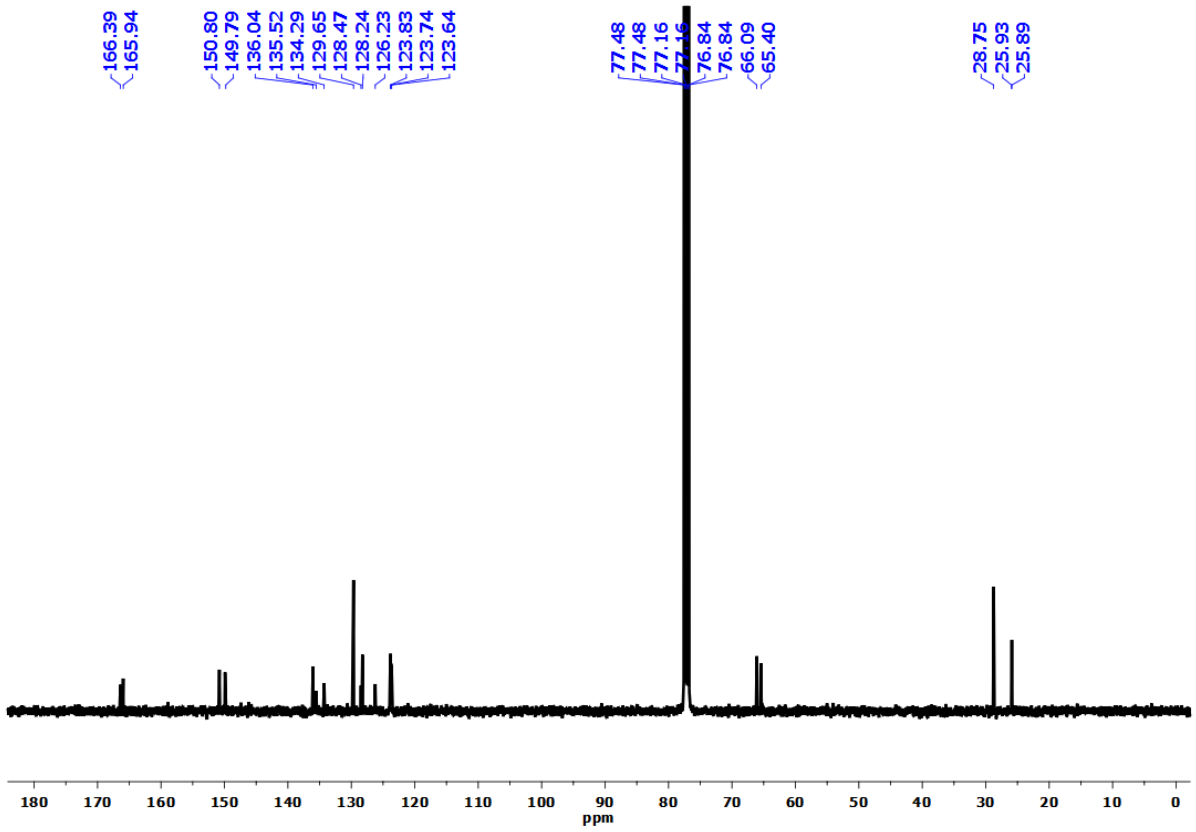

Figure 5S. ^{13}C-NMR spectrum of **L2** in $CDCl_3$ in 100 MHz at 298K.

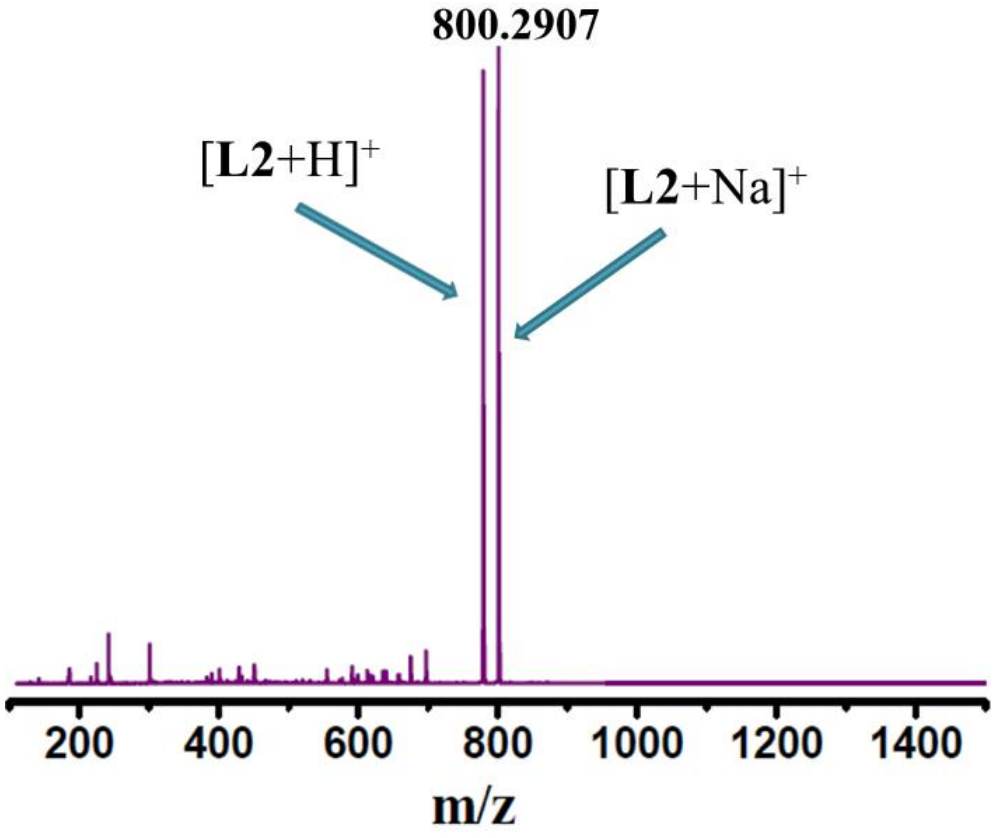

Figure 6S. ESI-MS(+ve) spectrum of **L2** at 298K.

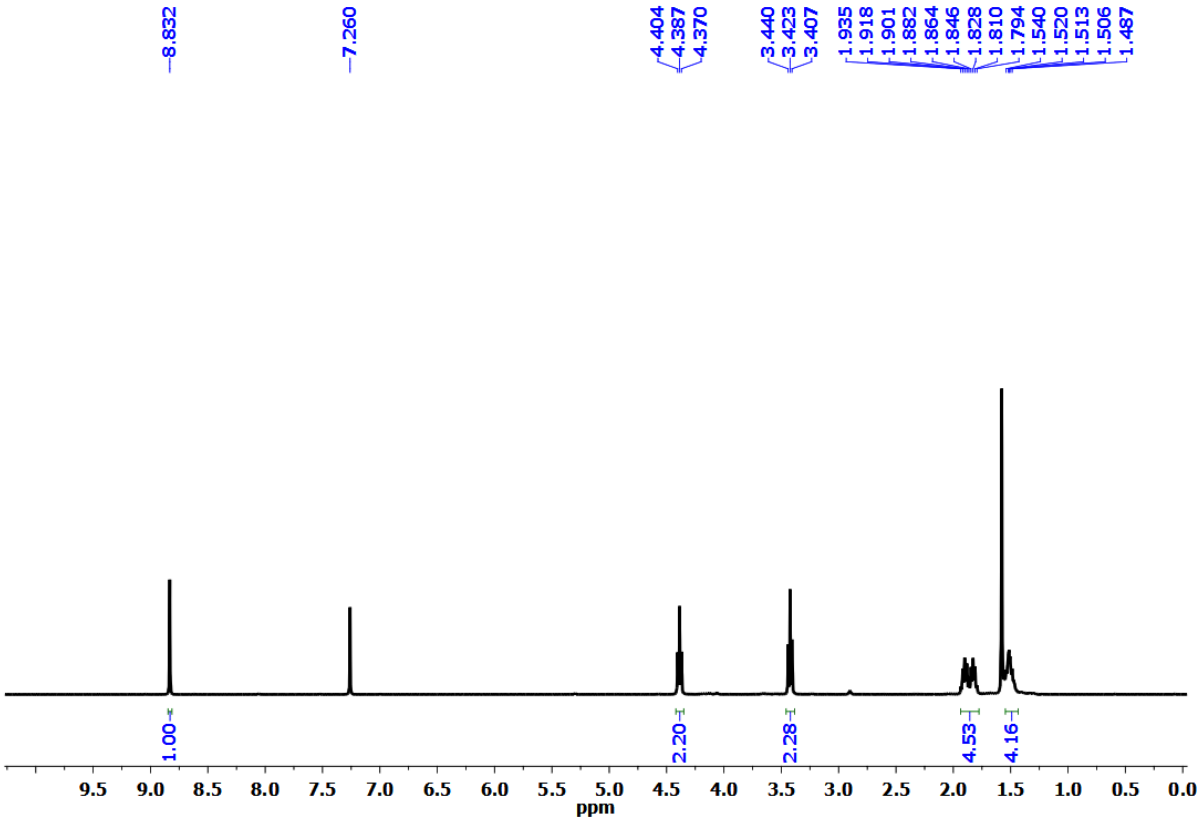

Figure 7S. ^{1}H-NMR spectrum of compound **B** in $CDCl_3$ in 400 MHz at 298K.

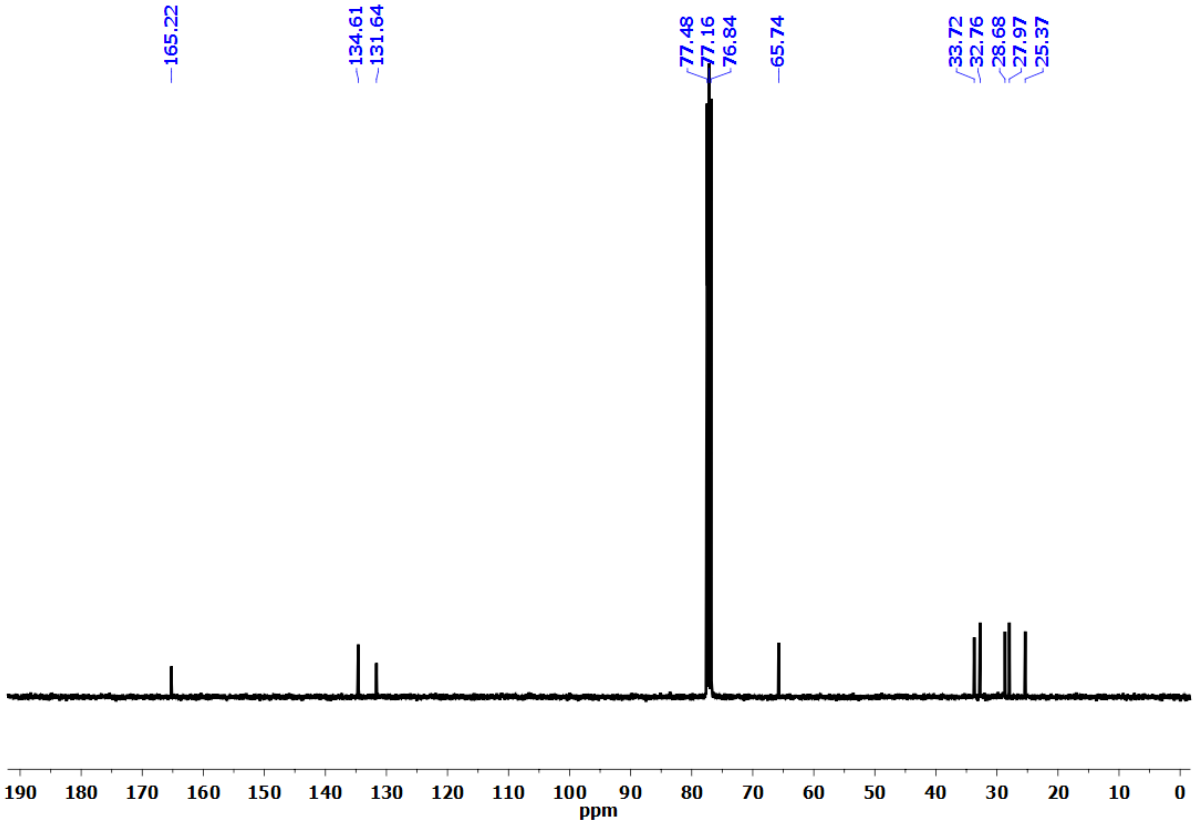

Figure 8S. ^{13}C-NMR spectrum of **B** in $CDCl_3$ in 100 MHz at 298K.

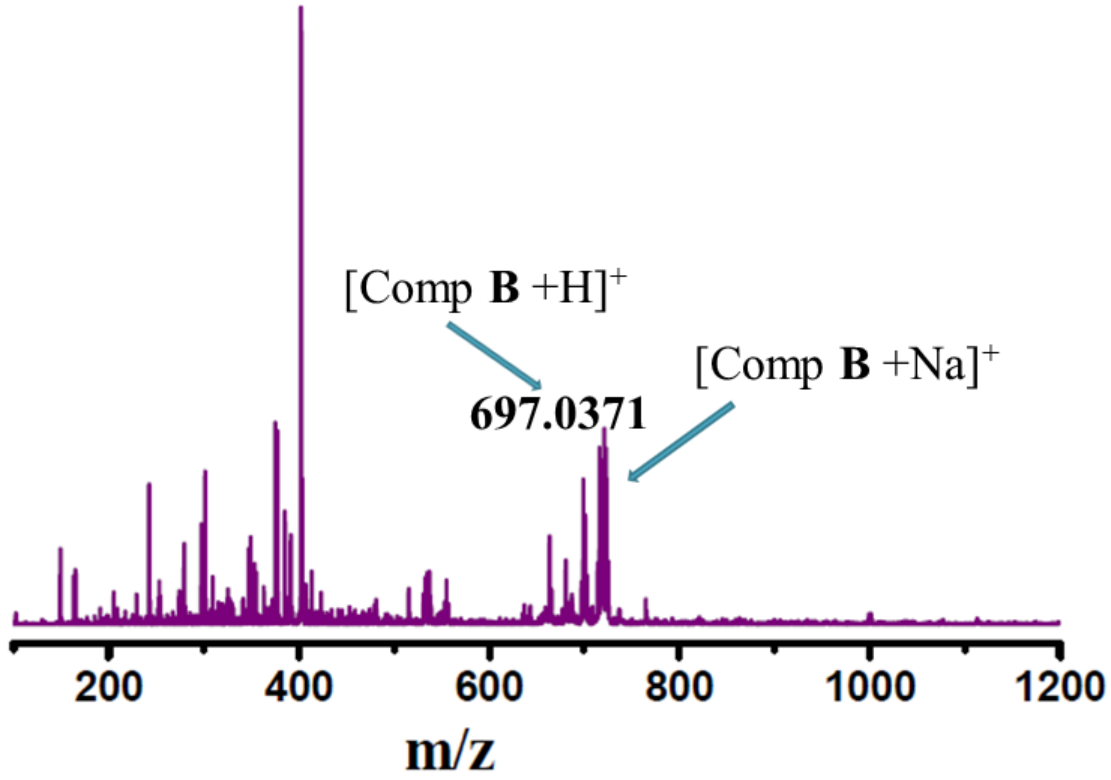

Figure 9S. ESI-MS(+ve) spectrum of compound **B** at 298K.

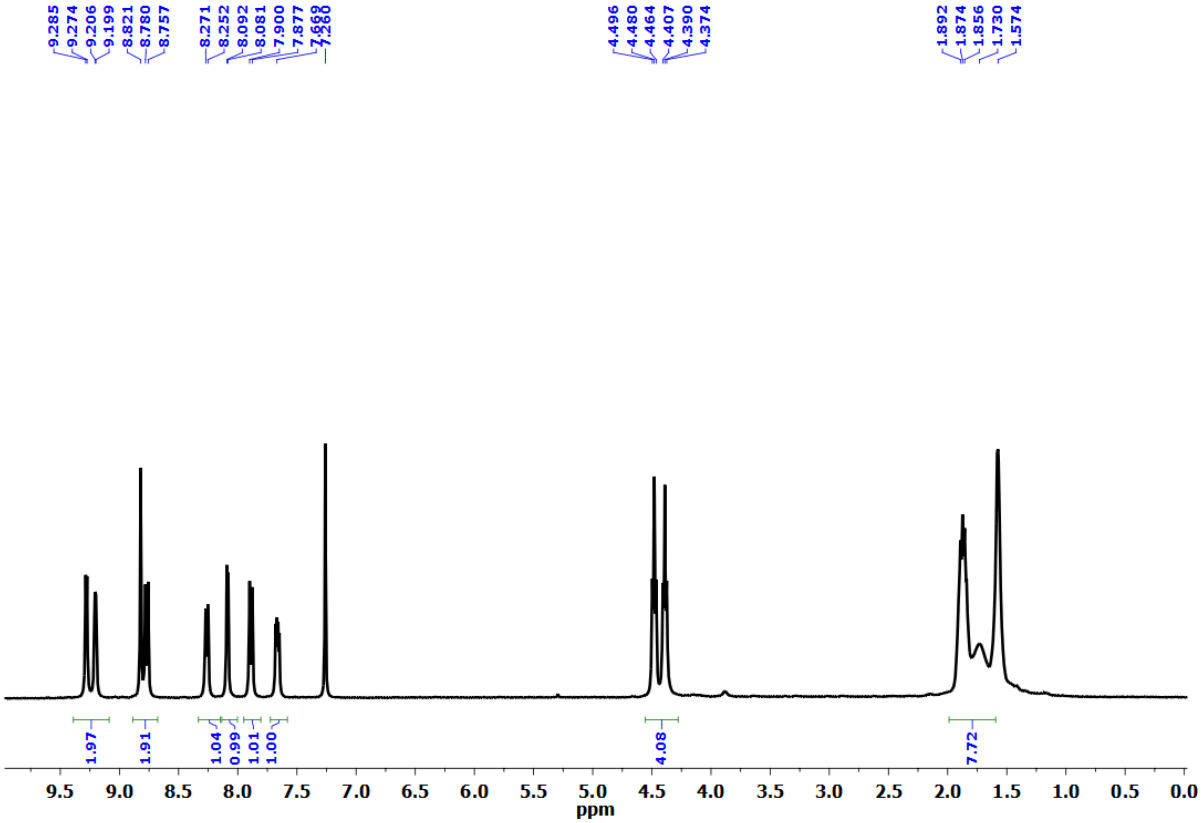

Figure 10S. ^{1}H-NMR spectrum of **L3** in $CDCl_3$ in 400 MHz at 298K.

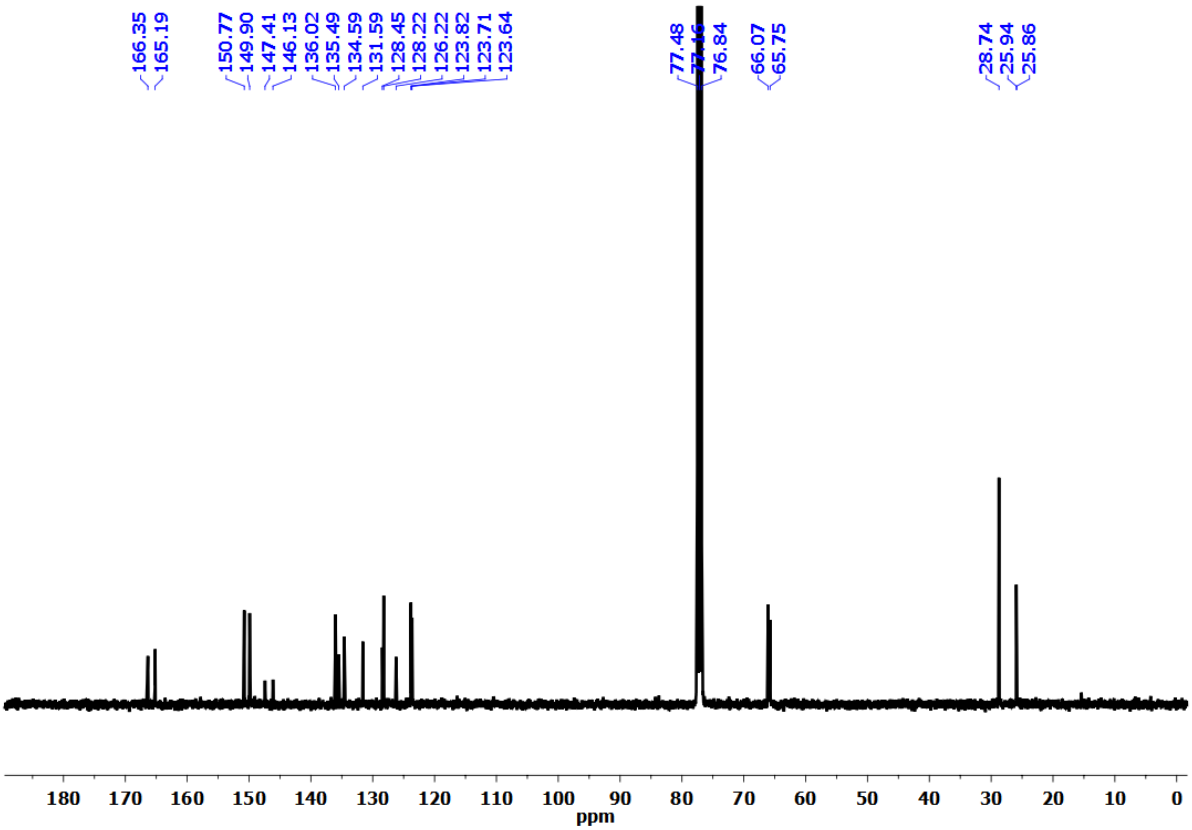

Figure 11S. ^{13}C-NMR spectrum of **L3** in $CDCl_3$ in 100 MHz at 298K.

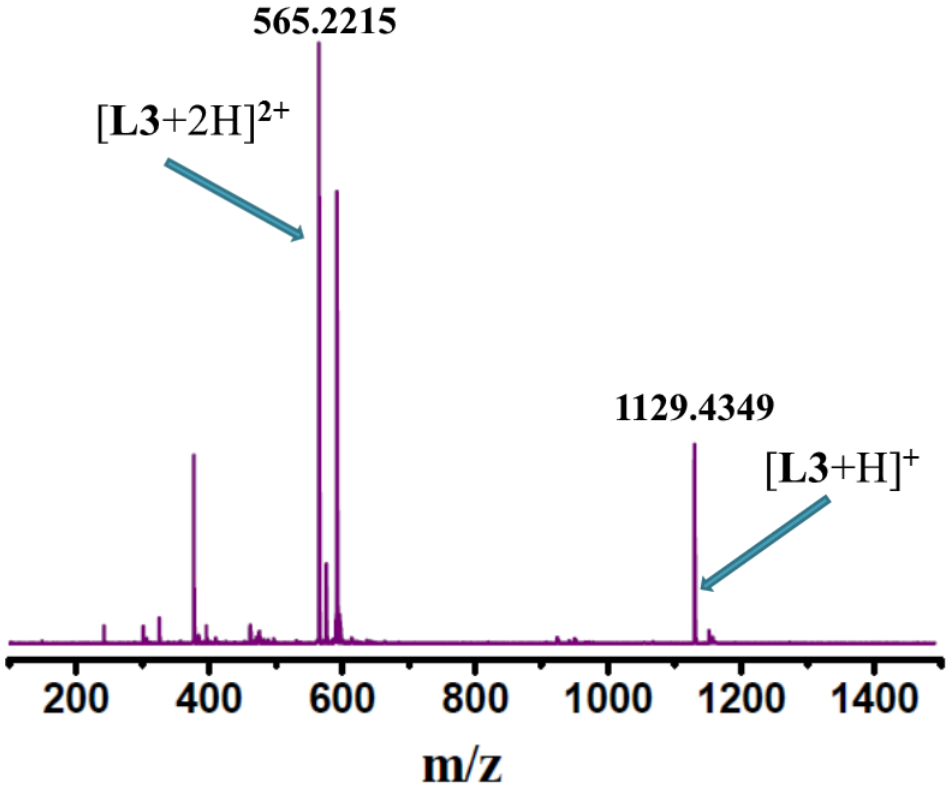

Figure 12S. ESI-MS(+ve) spectrum of **L3** at 298K.

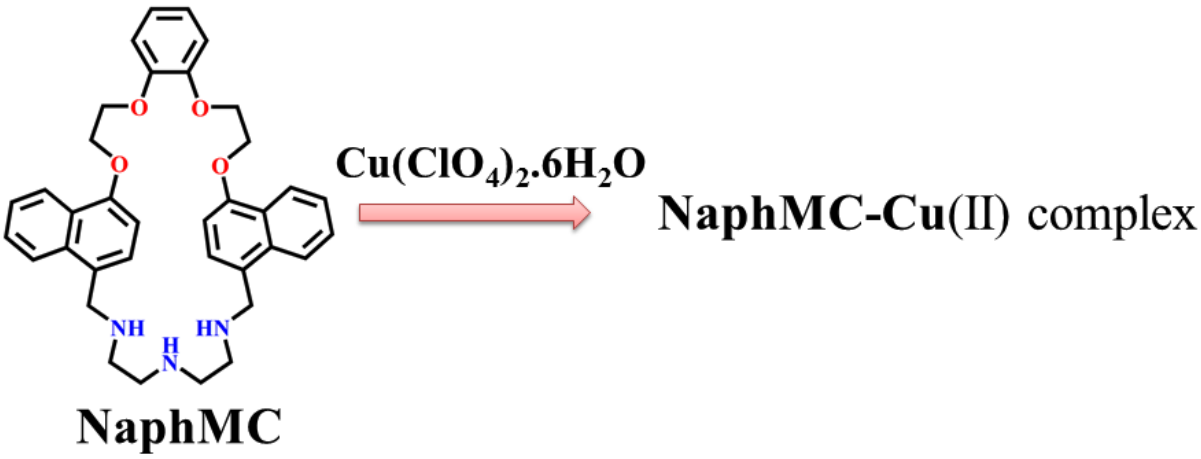

Scheme 3S. Synthetic route of **NaphMC-Cu**(II) complex

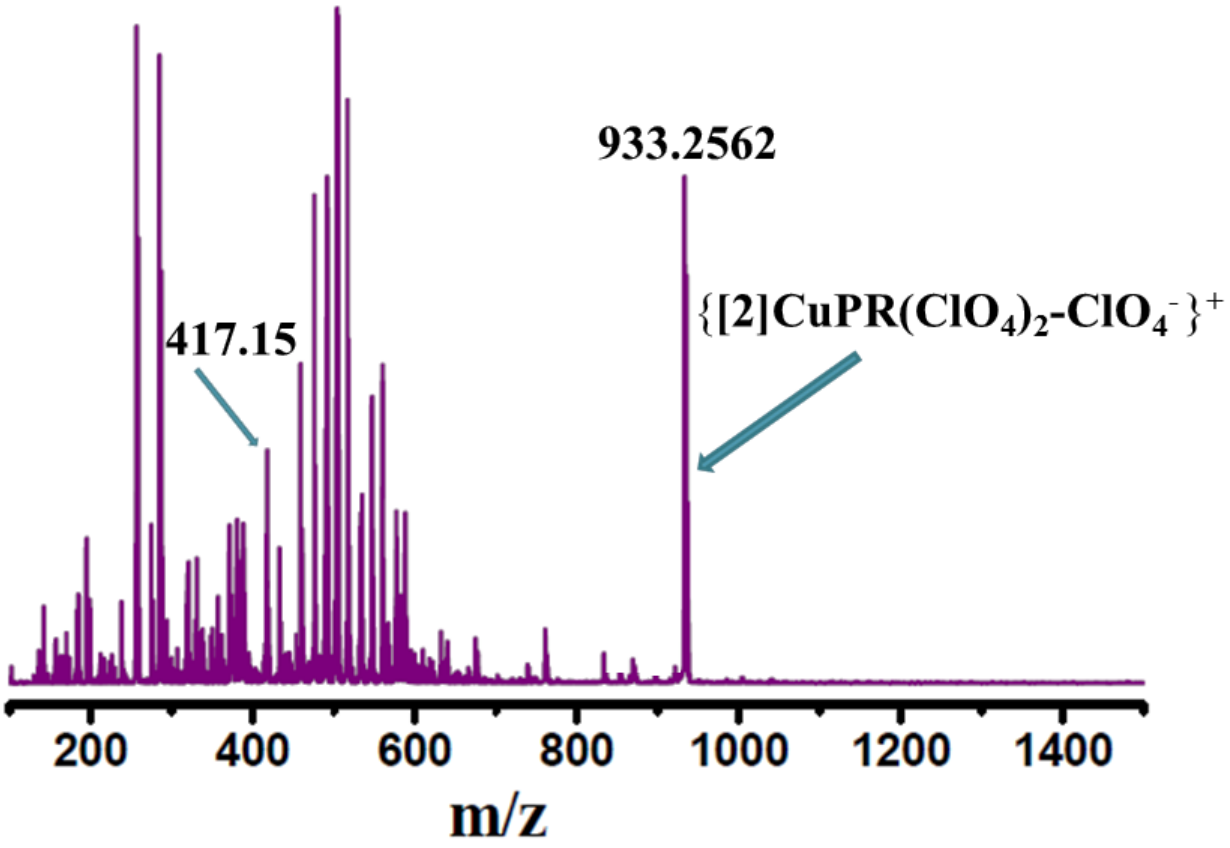

Figure 13S. ESI-MS(+ve) spectrum of **[2]CuPR(ClO$_4$)$_2$** at 298K.

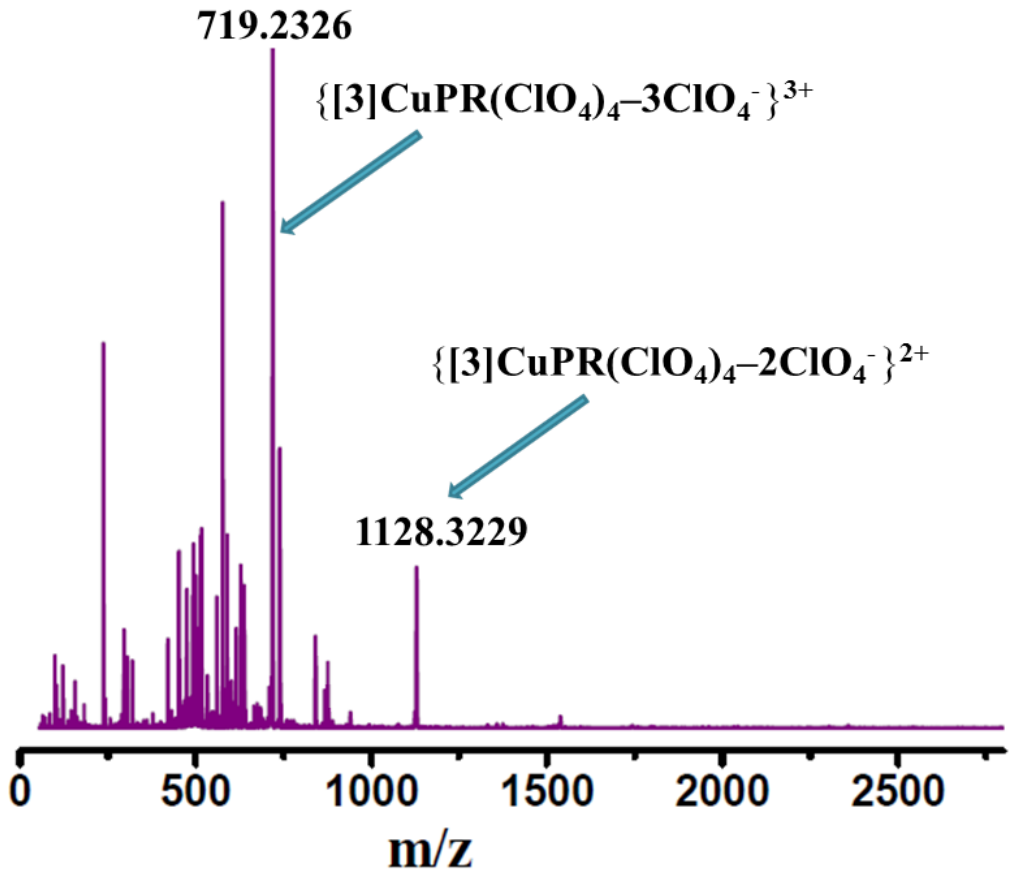

Figure 14S. ESI-MS(+ve) spectrum of **[3]CuPR(ClO$_4$)$_4$** at 298K.

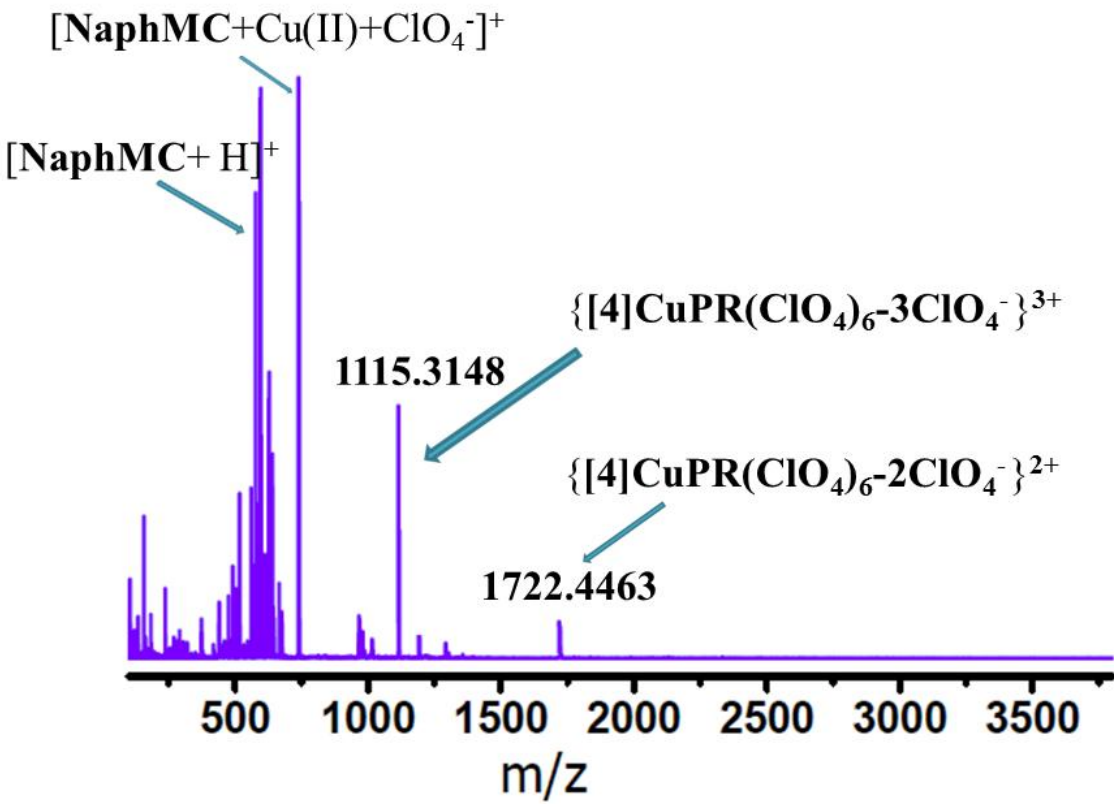

Figure 15S. ESI-MS(+ve) spectrum of **[4]CuPR(ClO$_4$)$_6$** at 298K.

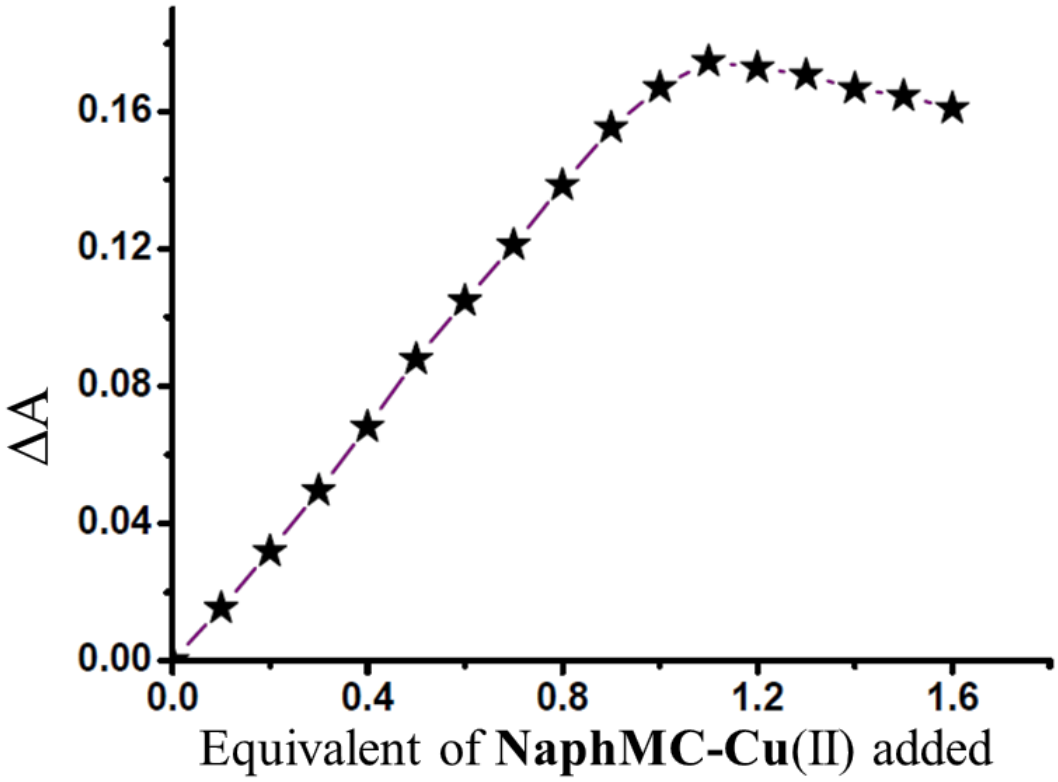

Figure 16S. Equivalence plot from UV/Vis titration experiment between **L1** and **NaphMC-Cu**(II) complex.

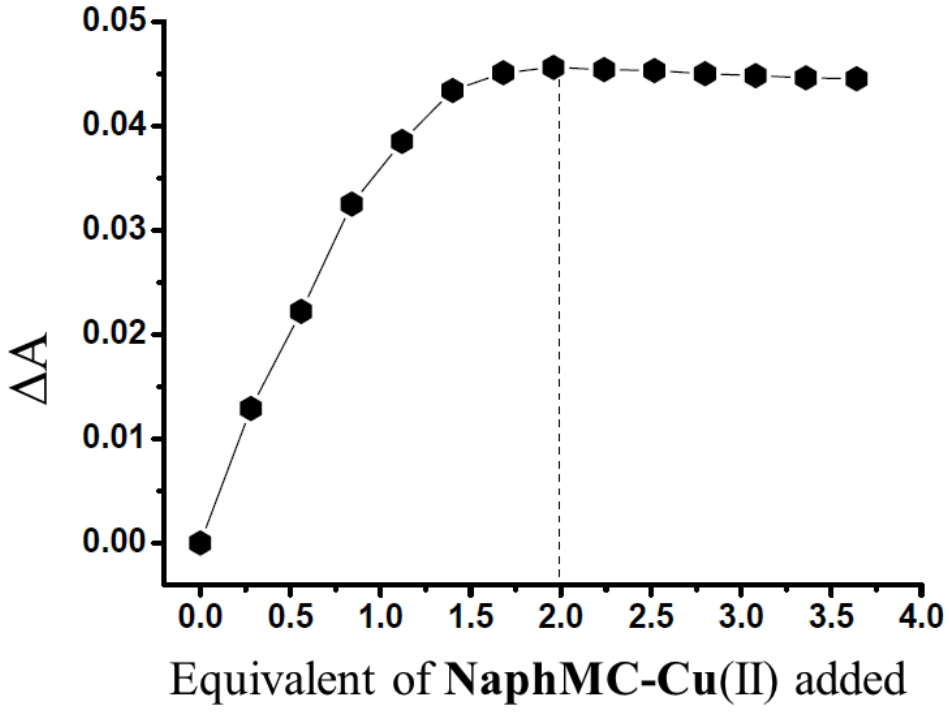

Figure 17S. Equivalence plot from UV/Vis titration experiment between **L2** and **NaphMC-Cu**(II) complex.

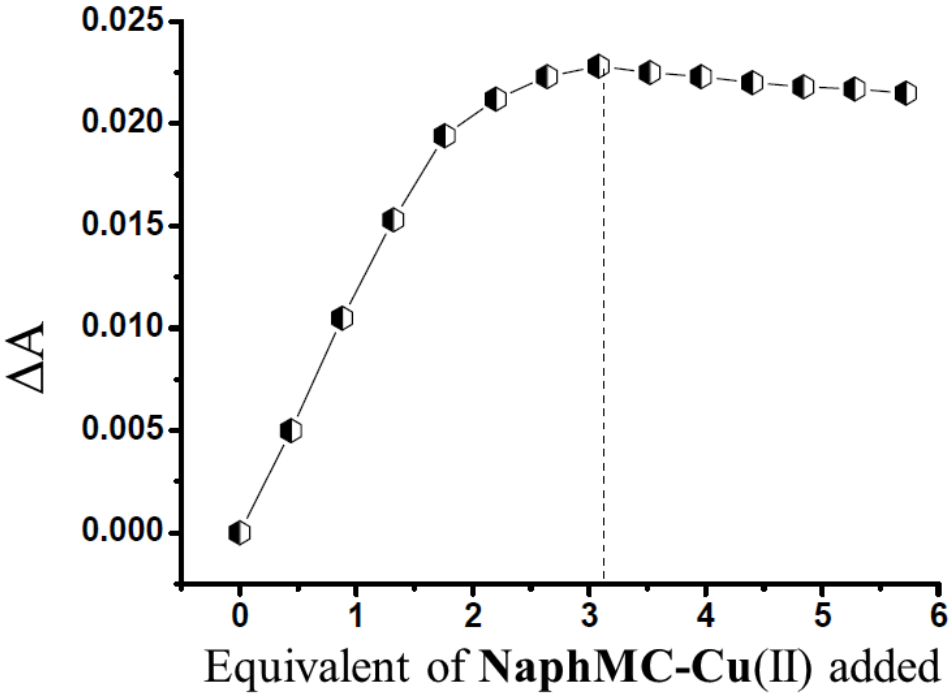

Figure 18S. Equivalence plot from UV/Vis titration experiment between **L3** and **NaphMC-Cu**(II) complex.

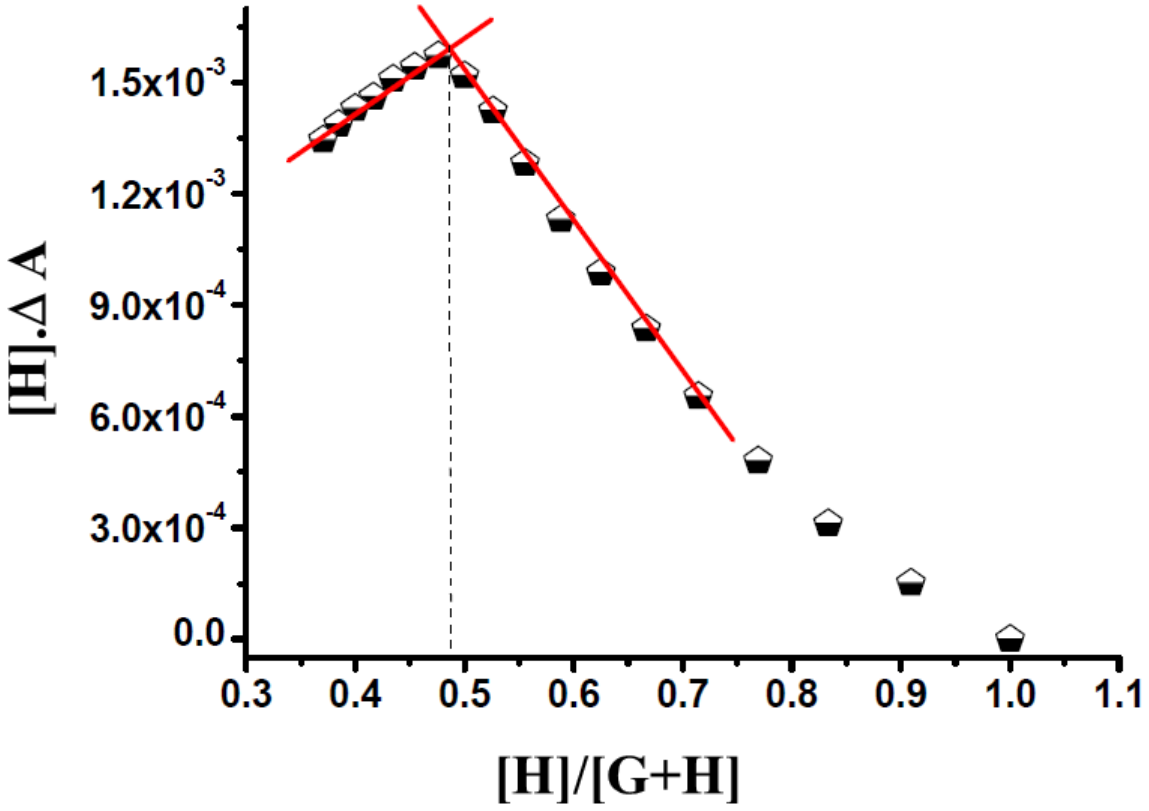

Figure 19S. Molar ratio plot from UV/Vis titration experiment between **Ll** with **NaphMC-Cu(II)** solution.

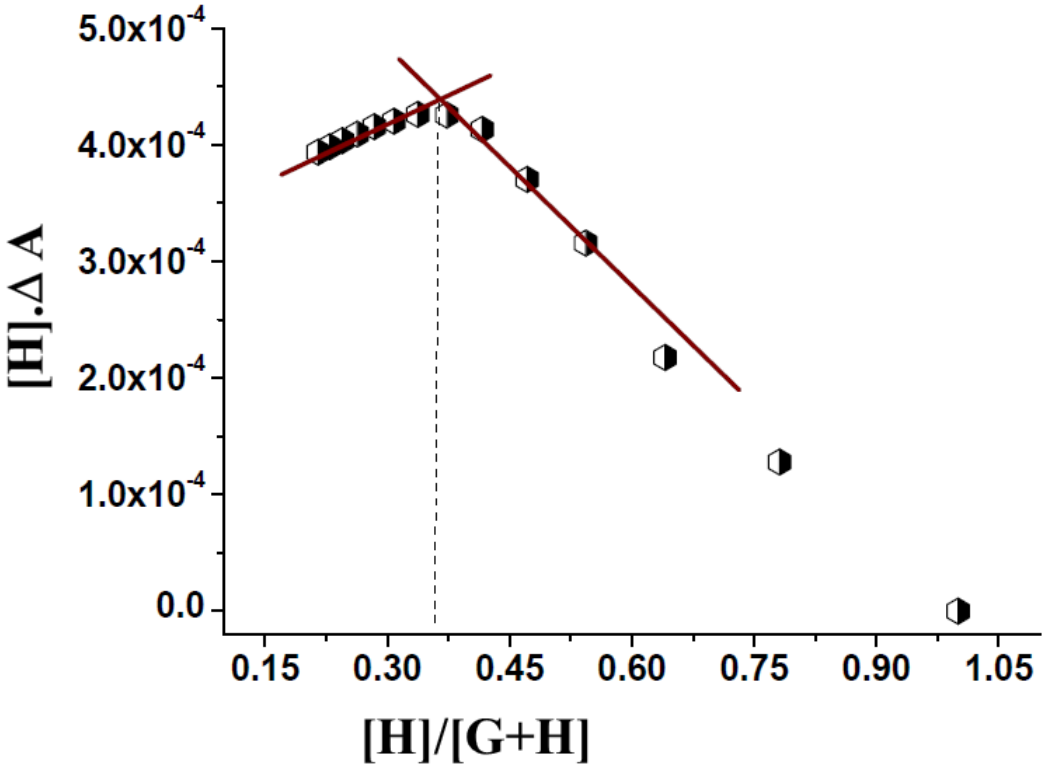

Figure 20S. Molar ratio plot from UV/Vis titration experiment between **L2** with **NaphMC-Cu(II)** solution.

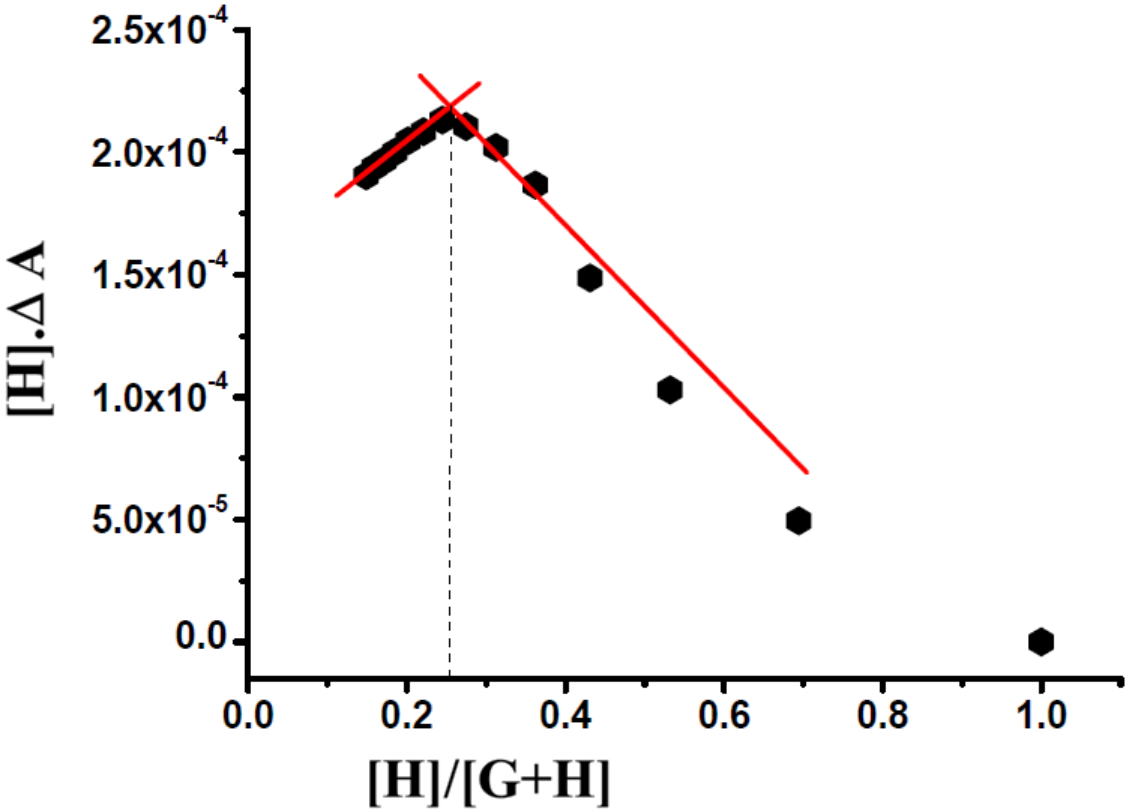

Figure 21S. Molar ratio plot from UV/Vis titration experiment between **L3** with **NaphMC-Cu(II)** solution.

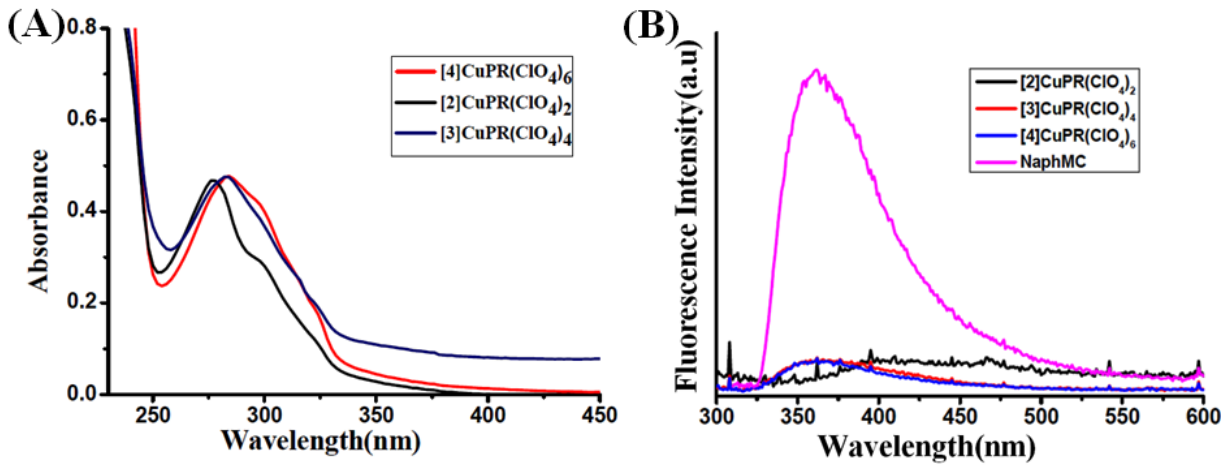

Figure 22S. Characteristic (A) UV/Vis and (B) emission spectra of pseudorotaxanes: **[2]CuPR(ClO$_4$)$_2$**, **[3]CuPR(ClO$_4$)$_4$** and **[4]CuPR(ClO$_4$)$_6$** in CH_3CN at 298K.

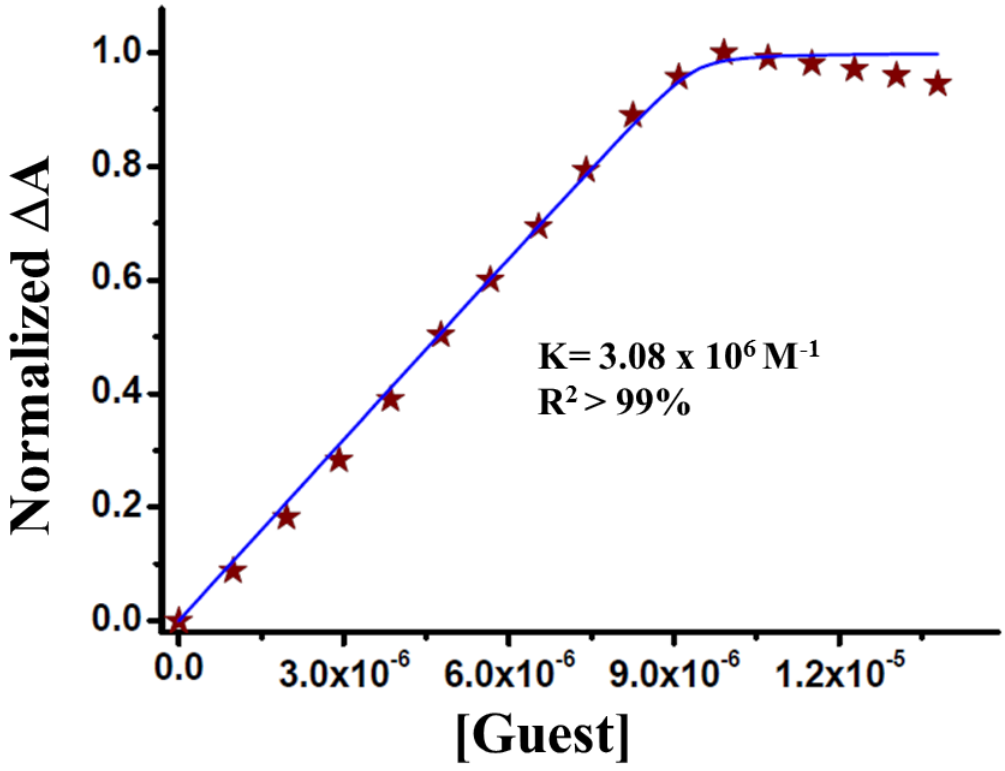

Figure 23S. Nonlinear 1:1 curve fitting to determine binding constant from UV/Vis titration experiment between **Ll** with **NaphMC-Cu(II)** solution.

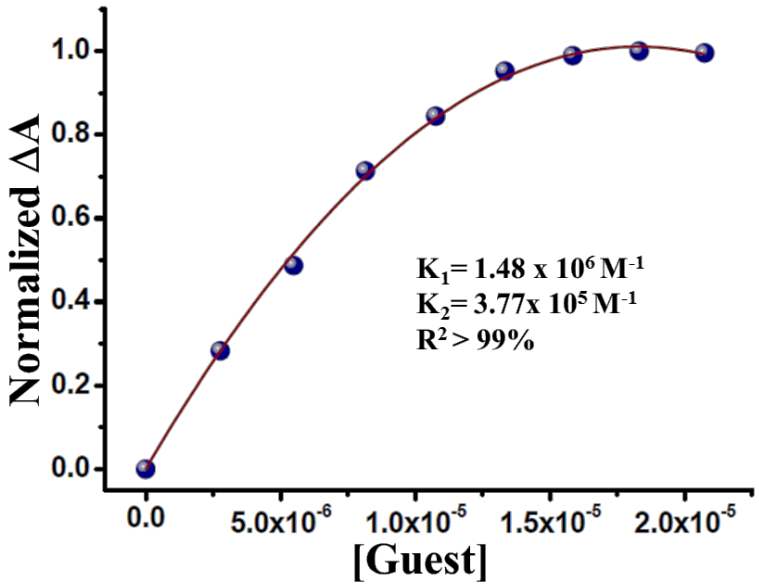

Figure 24S. Nonlinear 1:1 curve fitting to determine binding constant from UV/Vis titration experiment between **L2** with **NaphMC-Cu(II)** solution.

Crystallographic details of $([2]CuPR)^{2+}$

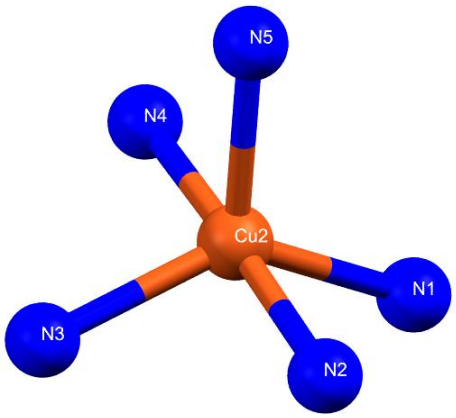

Figure 25S. Geometry around the **Cu**(II) center of **$([2]CuPR)^{2+}$** (τ = 0.638).

Table 1S . Crystallographic data of **([2]CuPR)$^{2+}$**

Compound	**[2]pseudorotaxane**
Formula	$C_{55}CuF_6H_{55}N_7O_{10}S_2$
$D_{calc.}$/ g cm^{-3}	1.498
μ/mm^{-1}	0.570
Formula Weight	1215.72
Colour	GREEN
Shape	block
Size/mm^3	0.06×0.03×0.02
T/K	127(2)
Crystal System	monoclinic
Flack Parameter	0.474(17)
Hooft Parameter	0.487(9)
Space Group	$P2_1$
a/Å	14.630(4)
b/Å	15.523(4)
c/Å	24.015(7)
α/°	90
β/°	98.701(9)
γ/°	90
V/Å^3	5391(2)
Z	4
Z'	2
Wavelength/Å	0.71073
Radiation type	MoK$_\alpha$
Θ_{min}/°	2.192
Θ_{max}/°	25.026
Measured Refl.	45000
Independent Refl.	18637
Reflections with I > 2(I)	14949
R_{int}	0.0917
Parameters	1488
Restraints	285
Largest Peak	0.661
Deepest Hole	-0.462
GooF	1.020
wR_2 (all data)	0.1909
wR_2	0.1748
R_1 (all data)	0.0851
R_1	0.0688
CCDC number	1892956

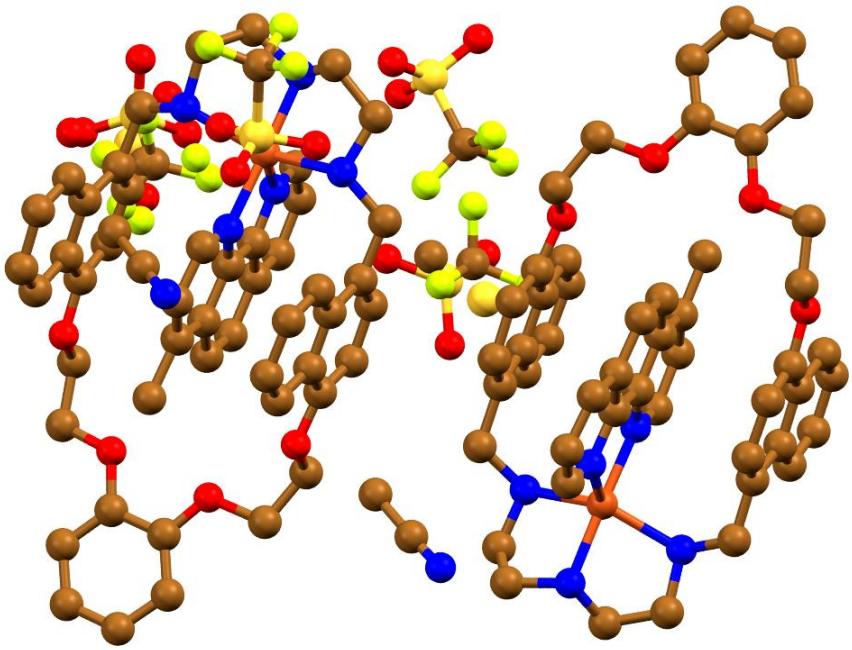

Figure 26S. Single Crystal X-ray structure of **([2]CuPR)$^{2+}$** (Ball and stick model). Hydrogen atoms are omitted for clarity.

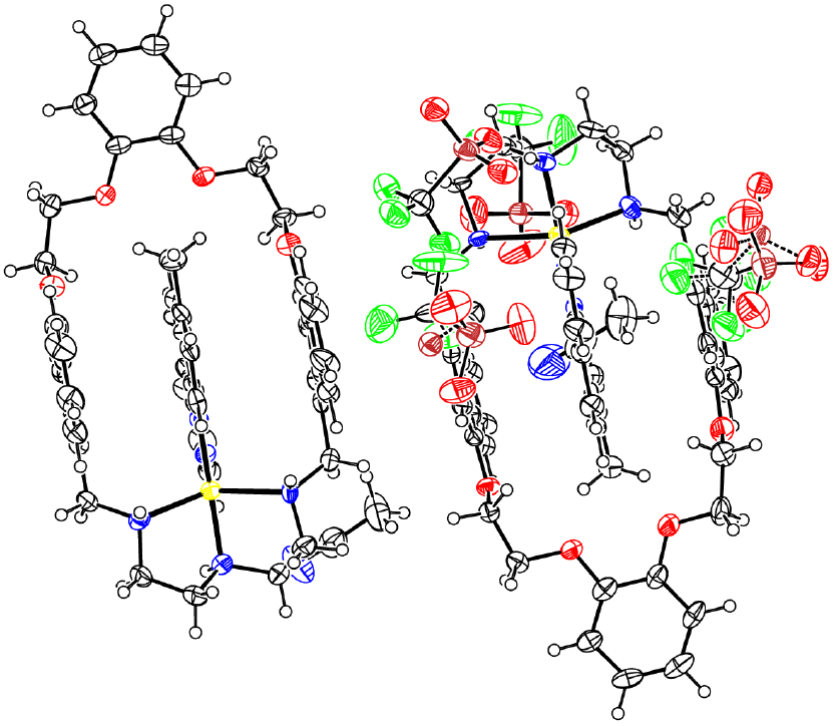

Figure 27S. Single Crystal X-ray structure of **([2]CuPR)$^{2+}$** (ellipsoid model using platon version).

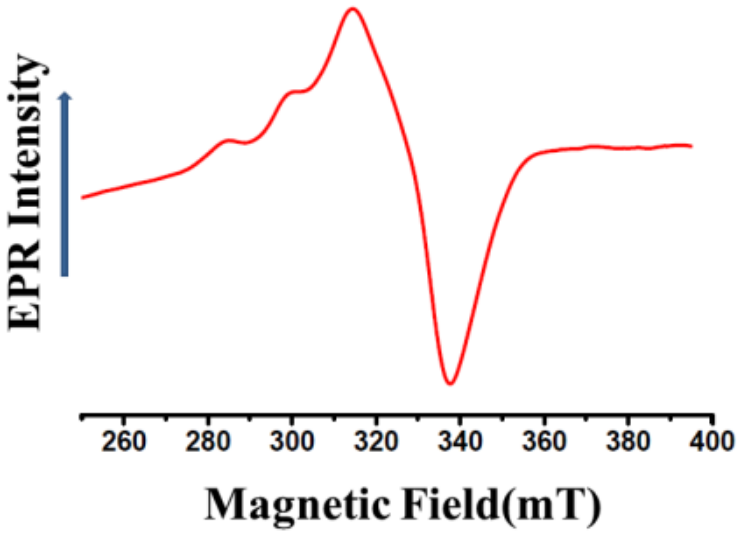

Figure 28S: EPR spectrum of **[2]CuPR(ClO_4)$_2$** in CH_3CN at 80K.

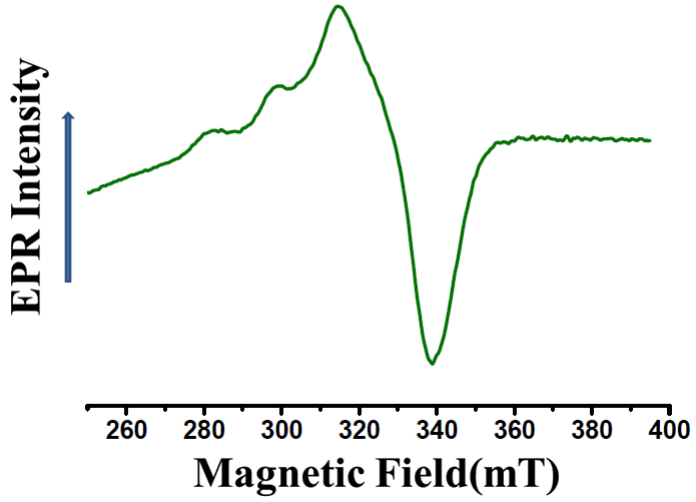

Figure 29S. EPR spectrum of **[3]CuPR(ClO_4)$_4$** in CH_3CN at 80K.

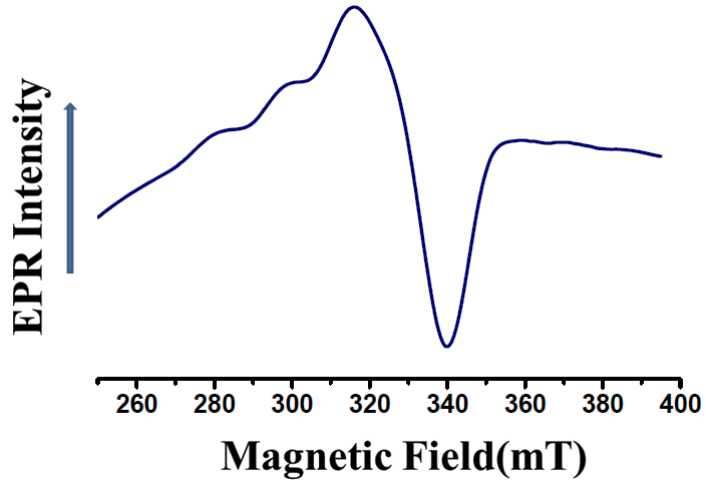

Figure 30S. EPR spectrum of **[4]CuPR(ClO_4)$_6$** in CH_3CN at 80K.

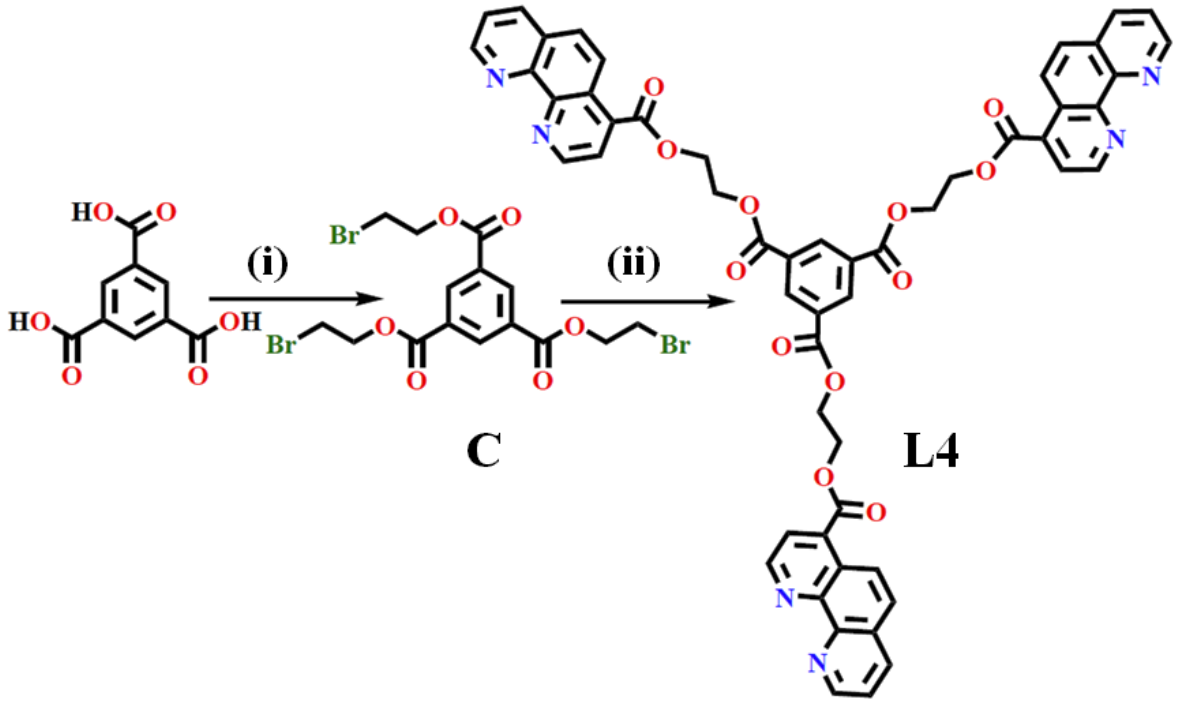

Scheme 4S: Synthetic route of axle **L4**; (i) 1,2-dibromoethane, K_2CO_3, DMF, RT, 20h, 86%, (ii) Phen-Acid, TBAF, THF, RT, 80 %.

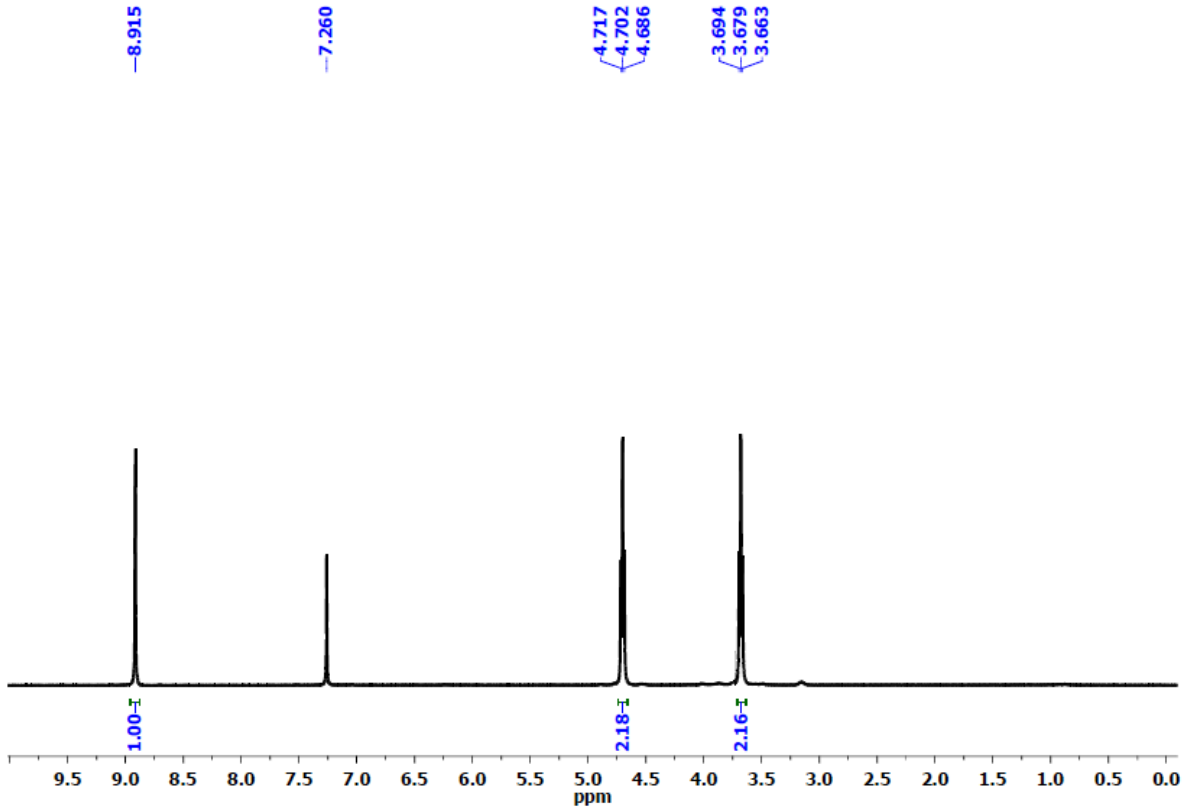

Figure 31S. ^{1}H-NMR spectrum of compound **C** in $CDCl_3$ in 400 MHz at 298K.

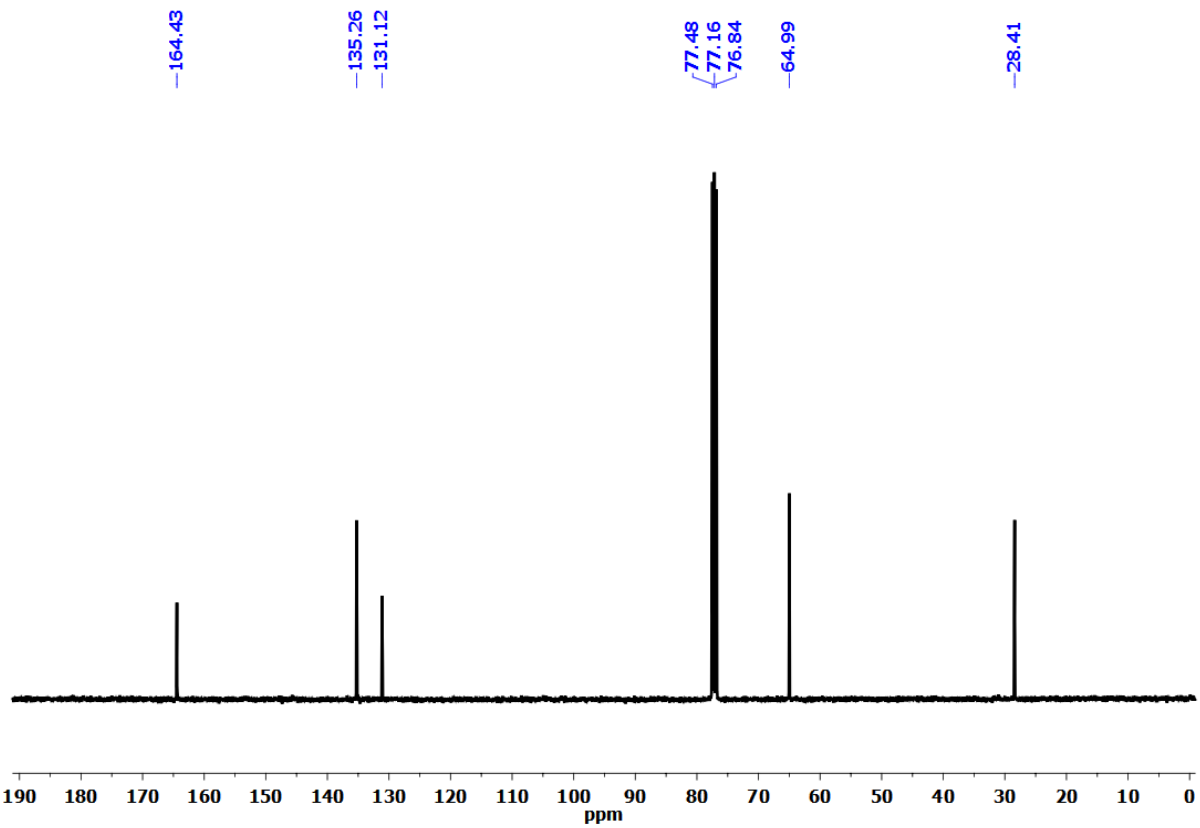

Figure 32S. ^{13}C-NMR spectrum of compound **C** in $CDCl_3$ in 100 MHz at 298K.

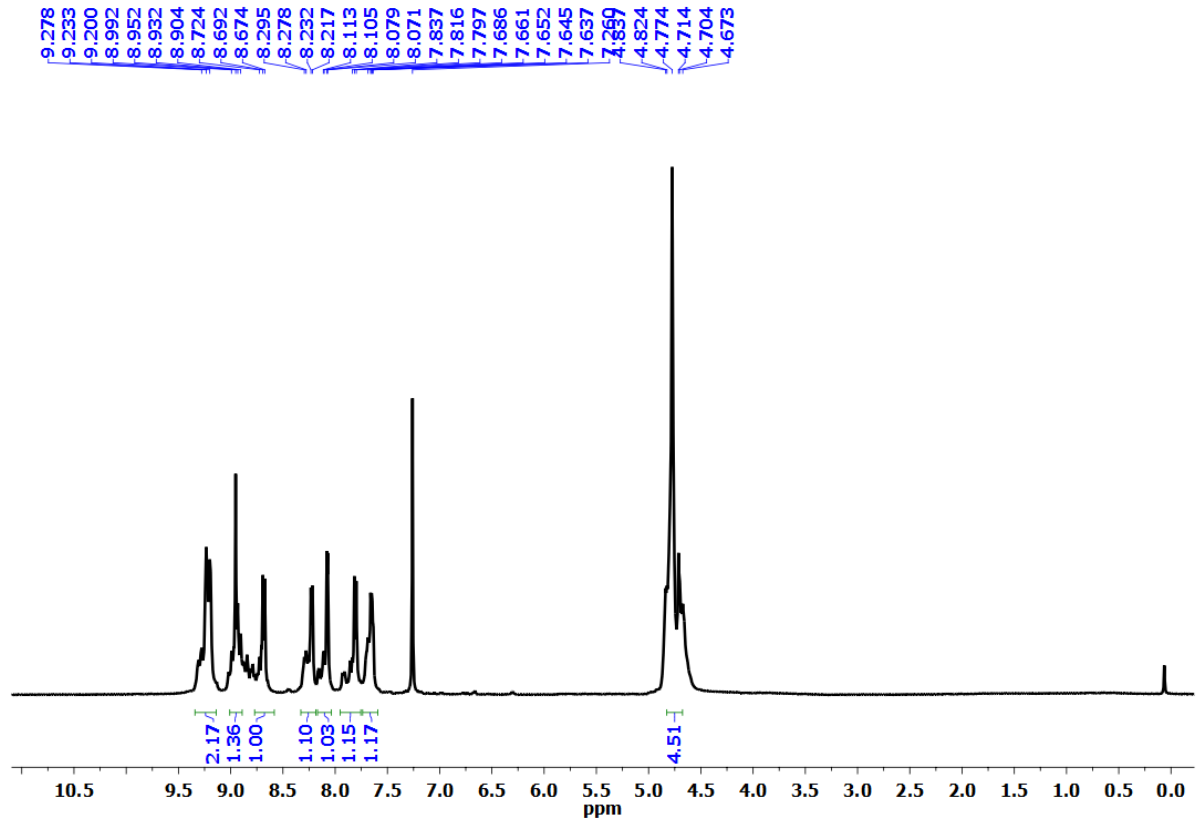

Figure 33S. ^{1}H-NMR spectrum of **L4** in $CDCl_3$ in 500 MHz at 298K.

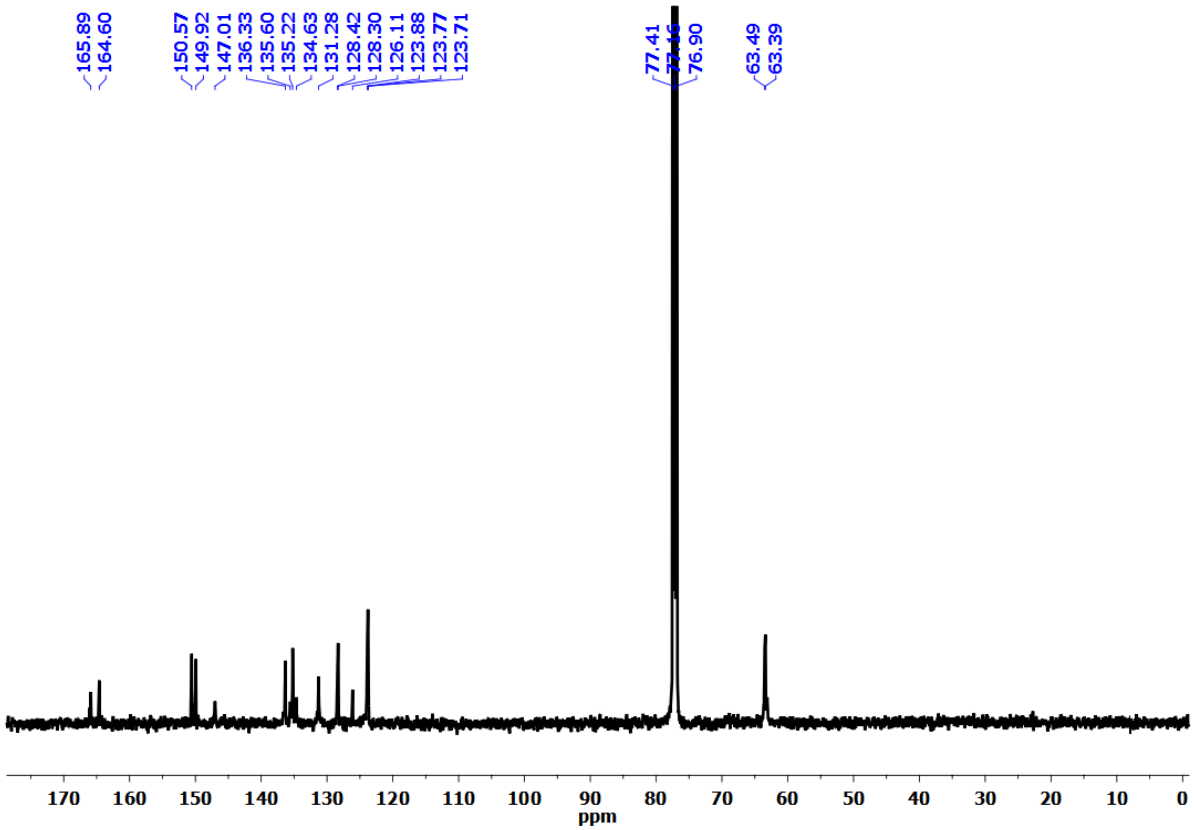

Figure 34S. ^{13}C-NMR spectrum of **L4** in $CDCl_3$ in 125 MHz at 298K.

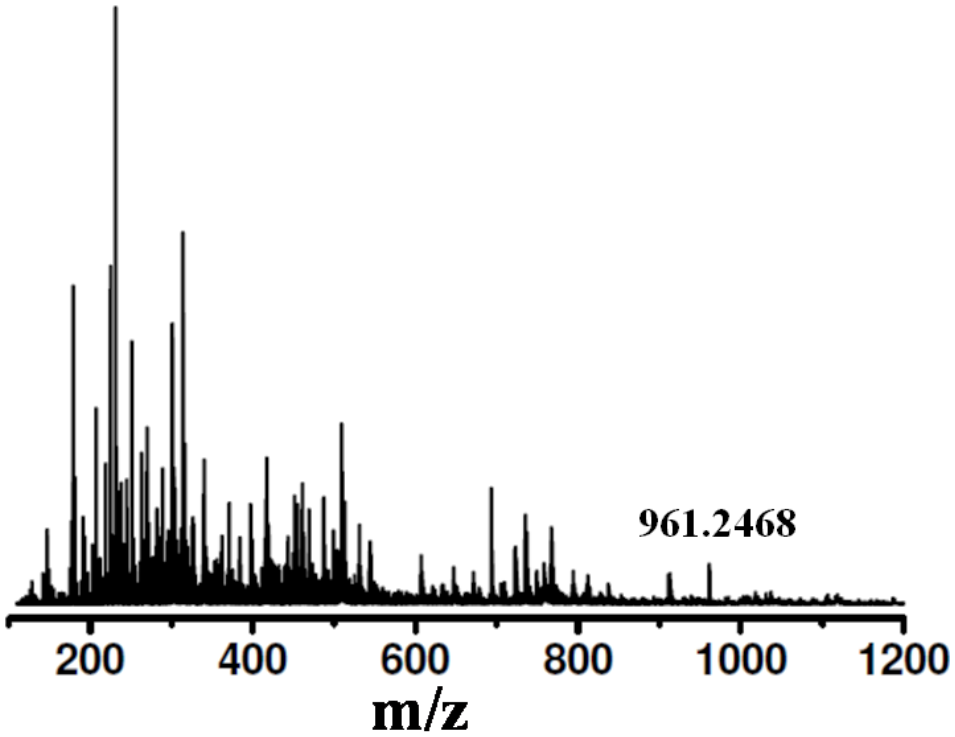

Figure 35S. ESI-MS(+ve) spectrum of **L4** at 298K.

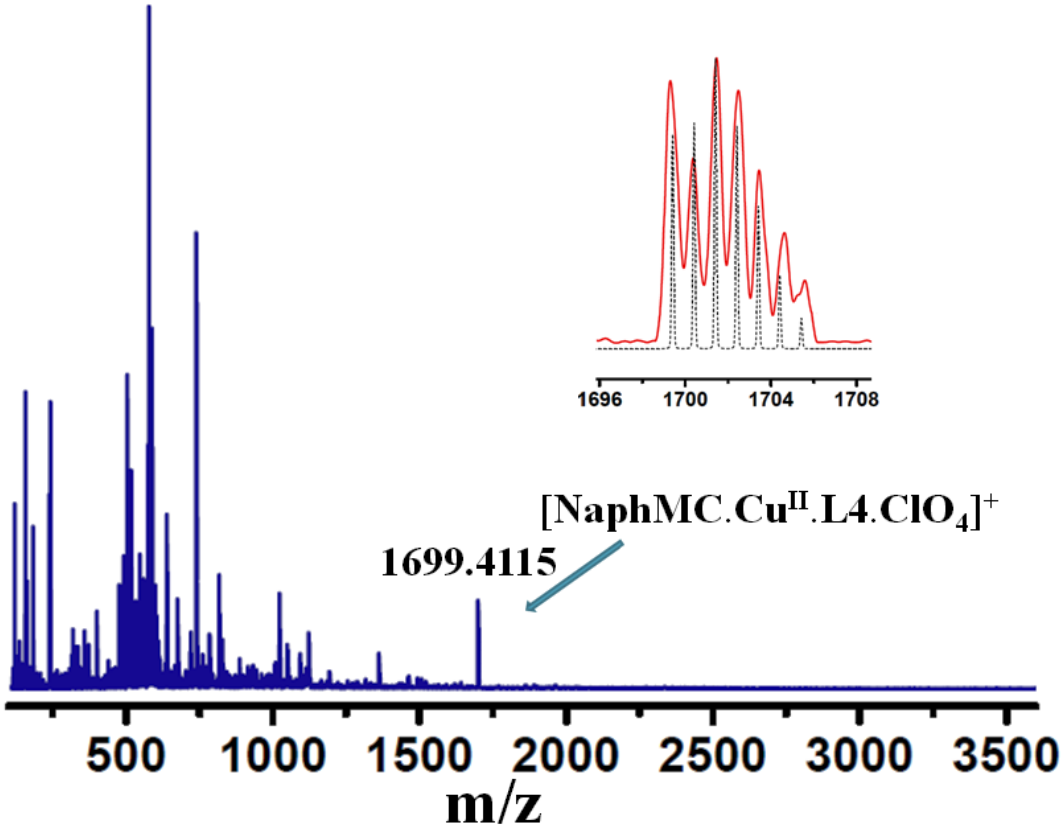

Figure 36S. ESI-MS(+ve) spectrum of **L4** axle based threaded molecule at 298K.

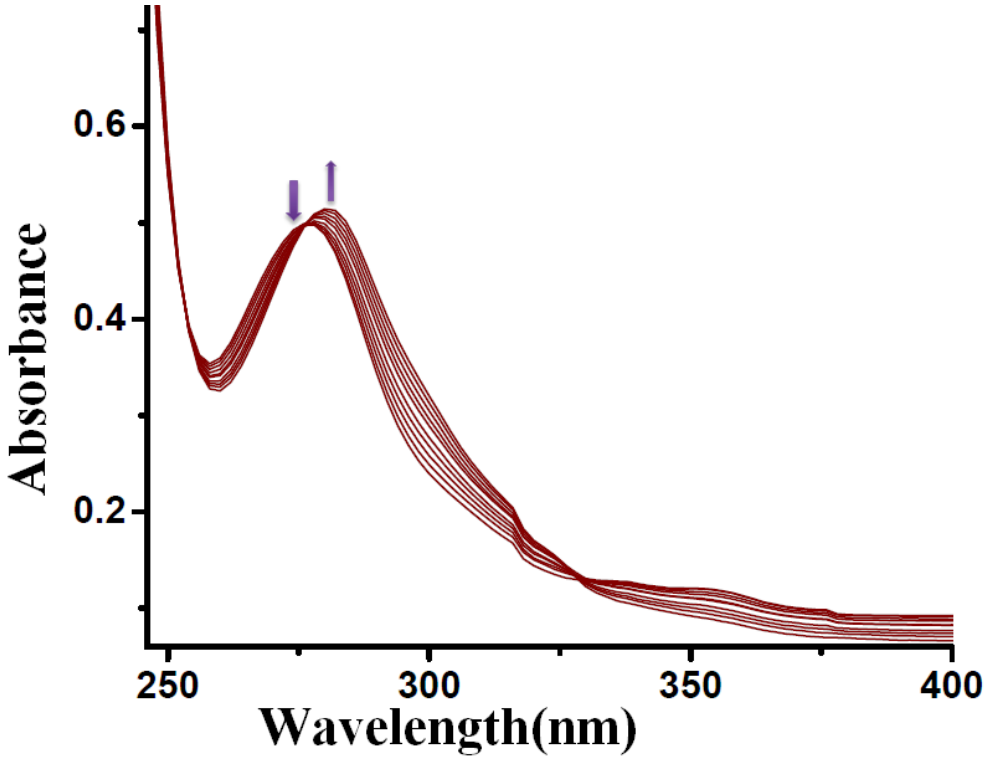

Figure 37S. UV/Vis titration profile between **L4** ($1x10^{-5}$ M) with **NaphMC-Cu**(II) ($1x10^{-4}$ M) in CH_3CN at 298 K.

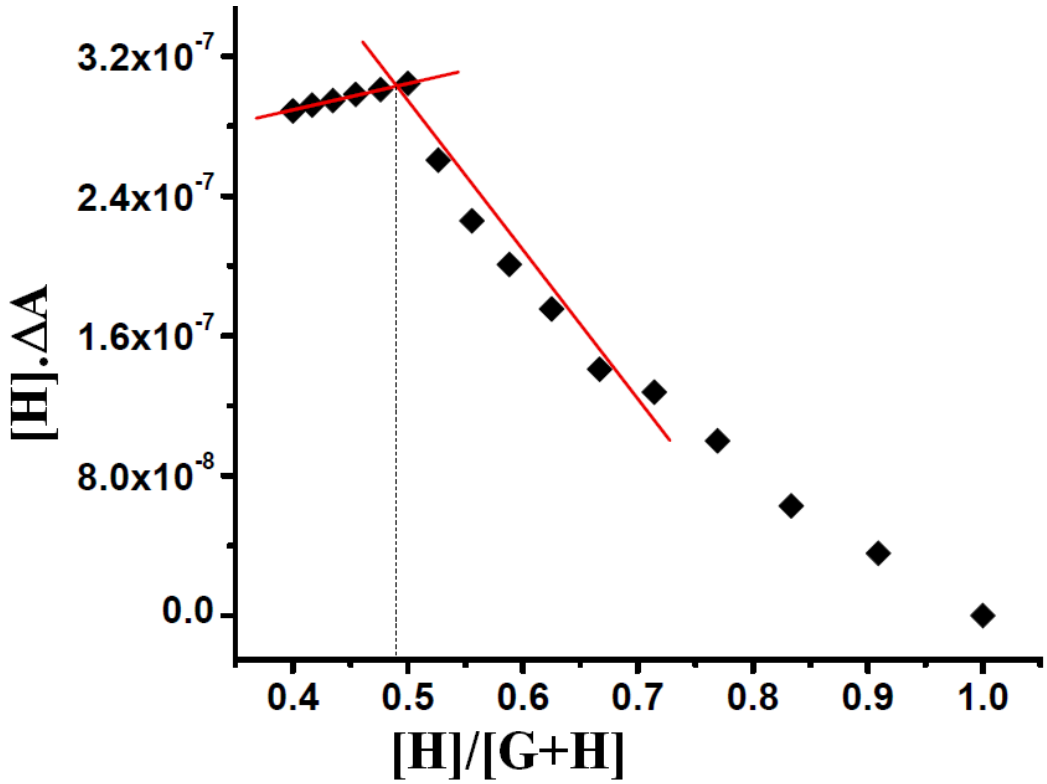

Figure 38S. Molar ratio plot from UV/Vis titration experiment between **L4** with **NaphMC-Cu(II)** solution.

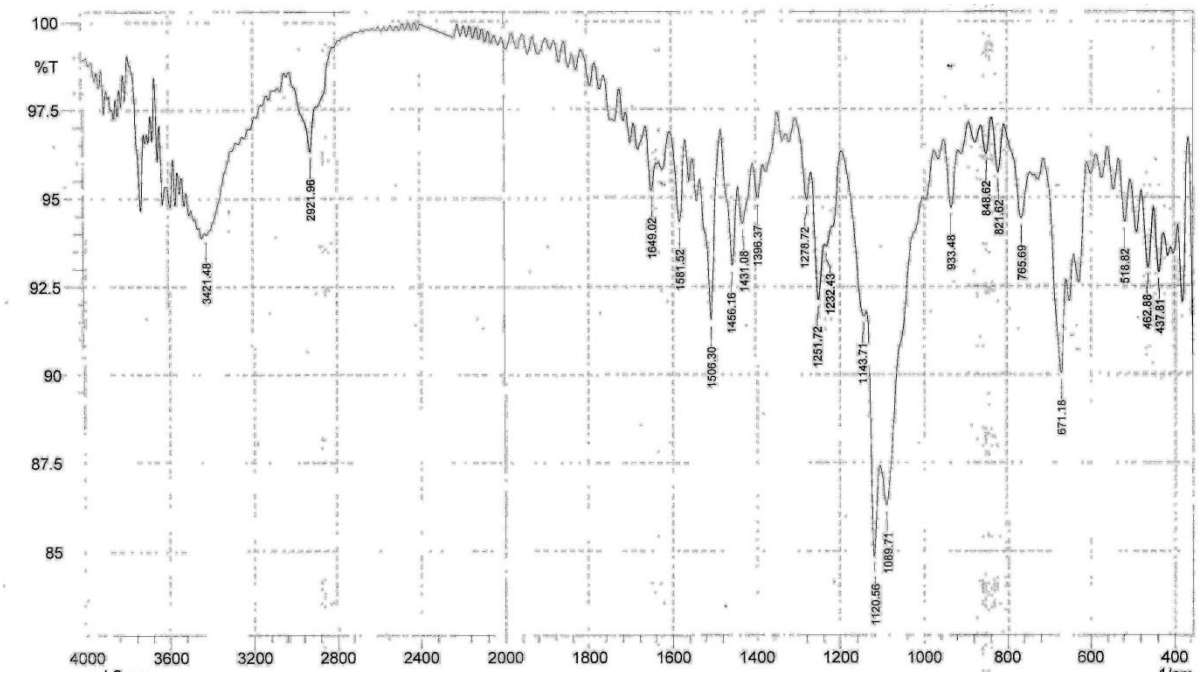

Figure 39S. FT-IR spectrum of **[2]CuPR(ClO$_4$)$_2$.**

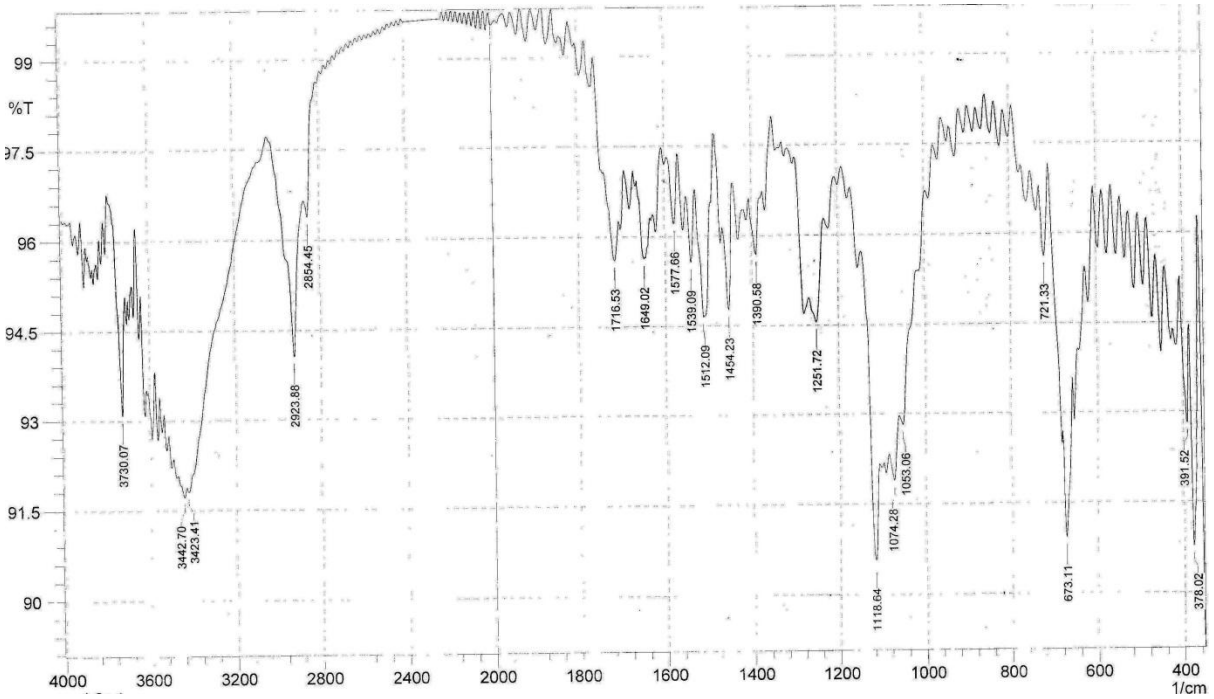

Figure 40S. FT-IR spectrum of **[3]CuPR(ClO$_4$)$_4$**.

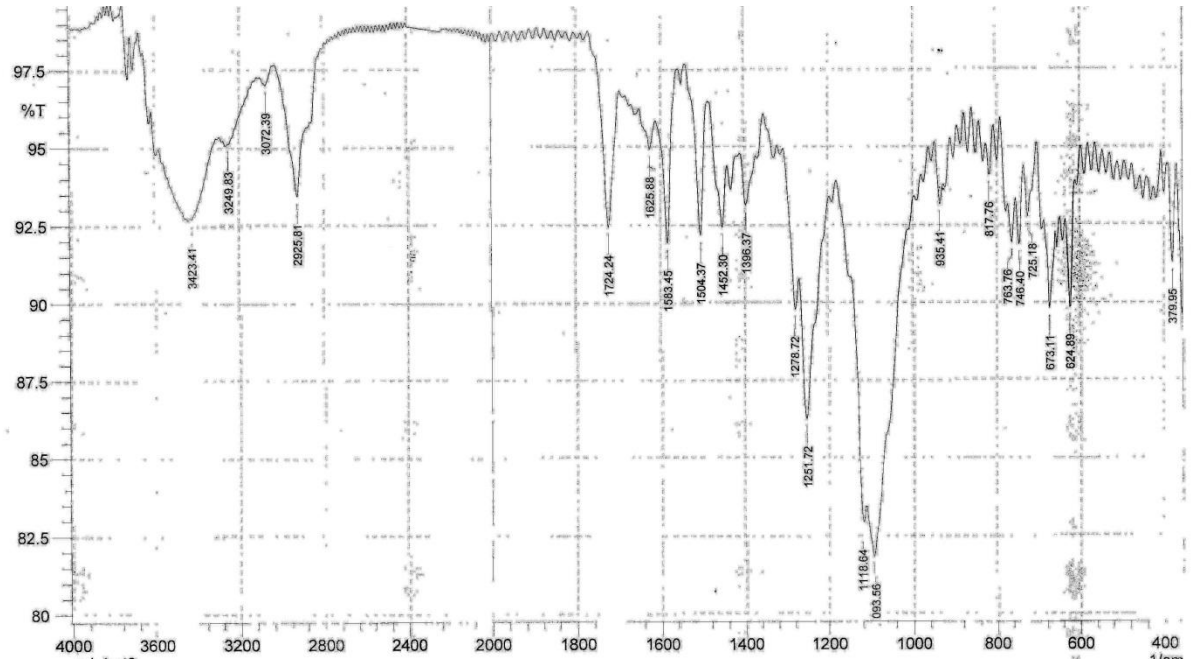

Figure 41S. FT-IR spectrum of **[4]CuPR(ClO$_4$)$_6$**.

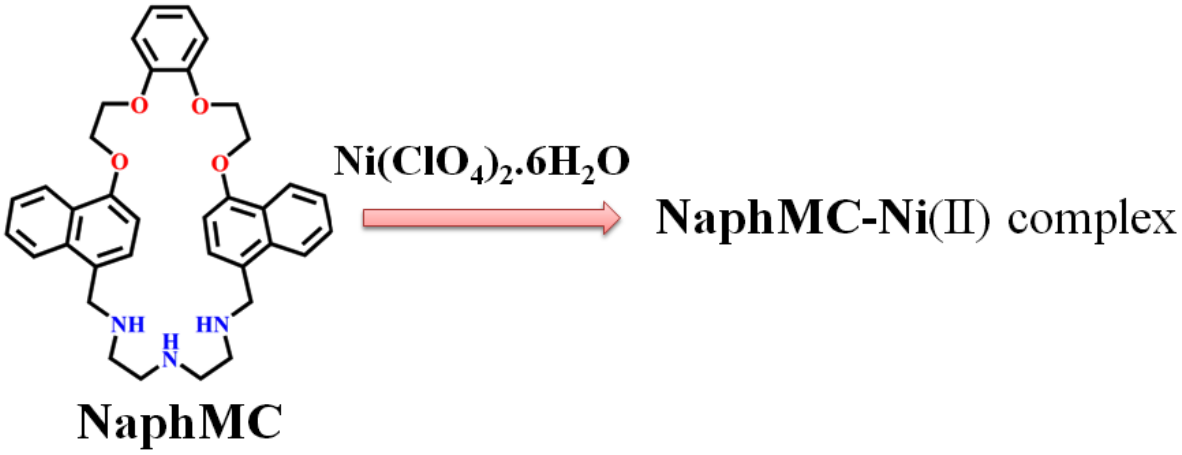

Scheme 5S. Synthetic route of **NaphMC-Ni**(II) complex

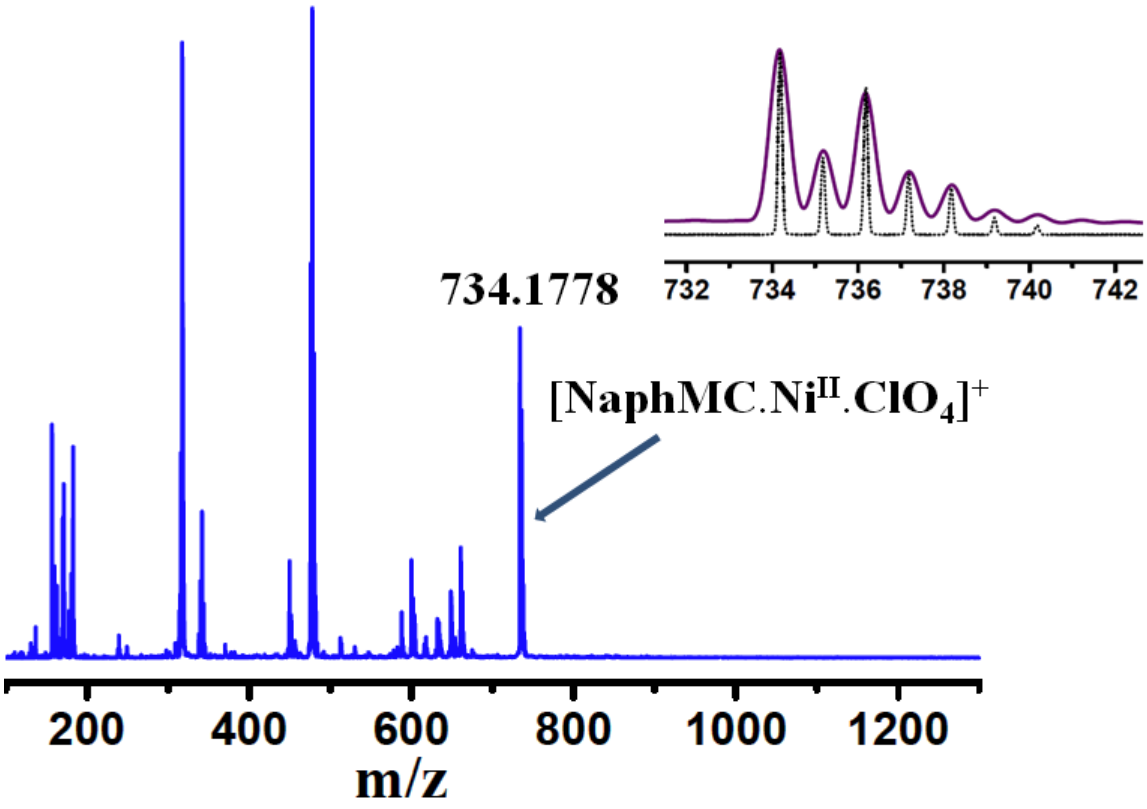

Figure 42S. ESI-MS(+ve) spectrum of **NaphMC-Ni**(II) complex at 298K.

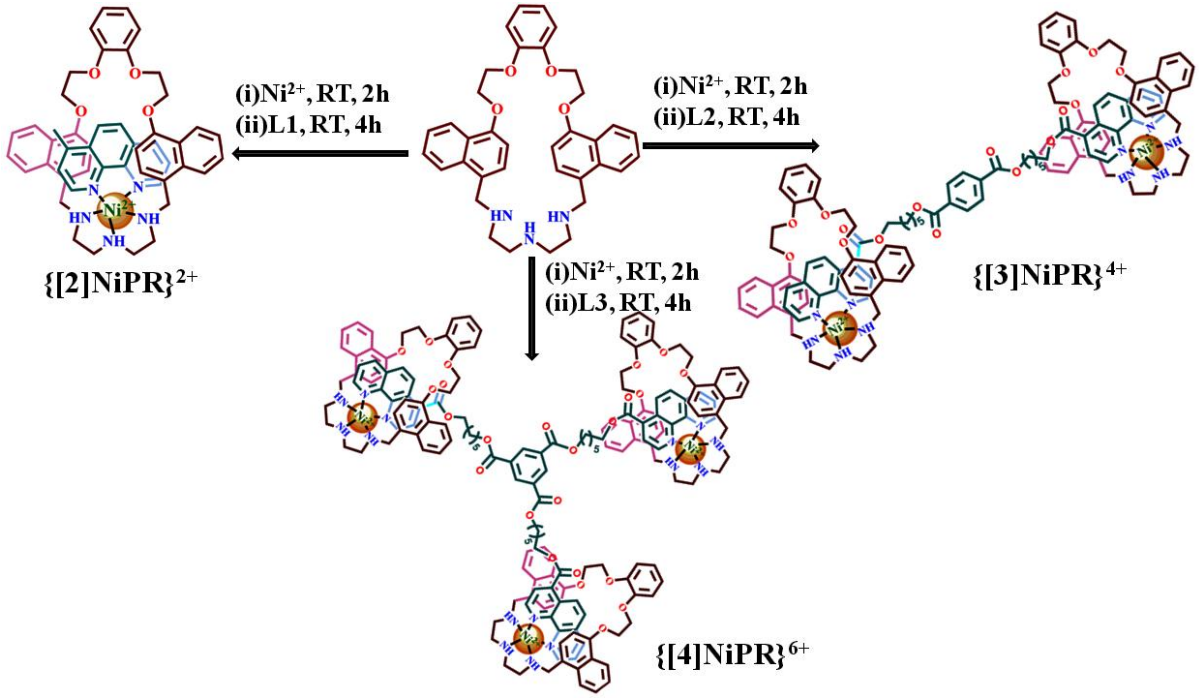

Scheme 6S. Synthetic route of formation of [2], [3], [4]pseudorotaxanes **{([2]NiPR)$^{2+}$, ([3]NiPR)$^{4+}$** and **([4]NiPR)$^{6+}$}**. Counter anions (ClO_4^-) are omitted for clarity.

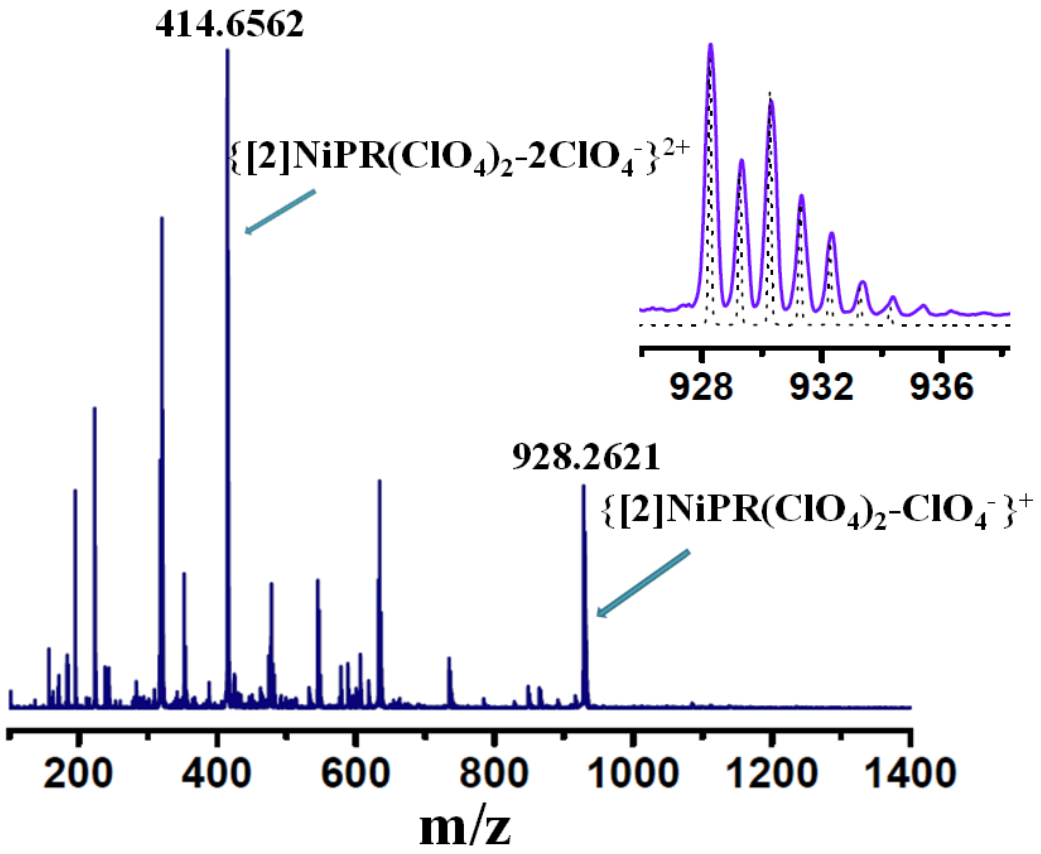

Figure 43S. ESI-MS(+ve) spectrum of **[2]NiPR(ClO$_4$)$_2$** at 298K.

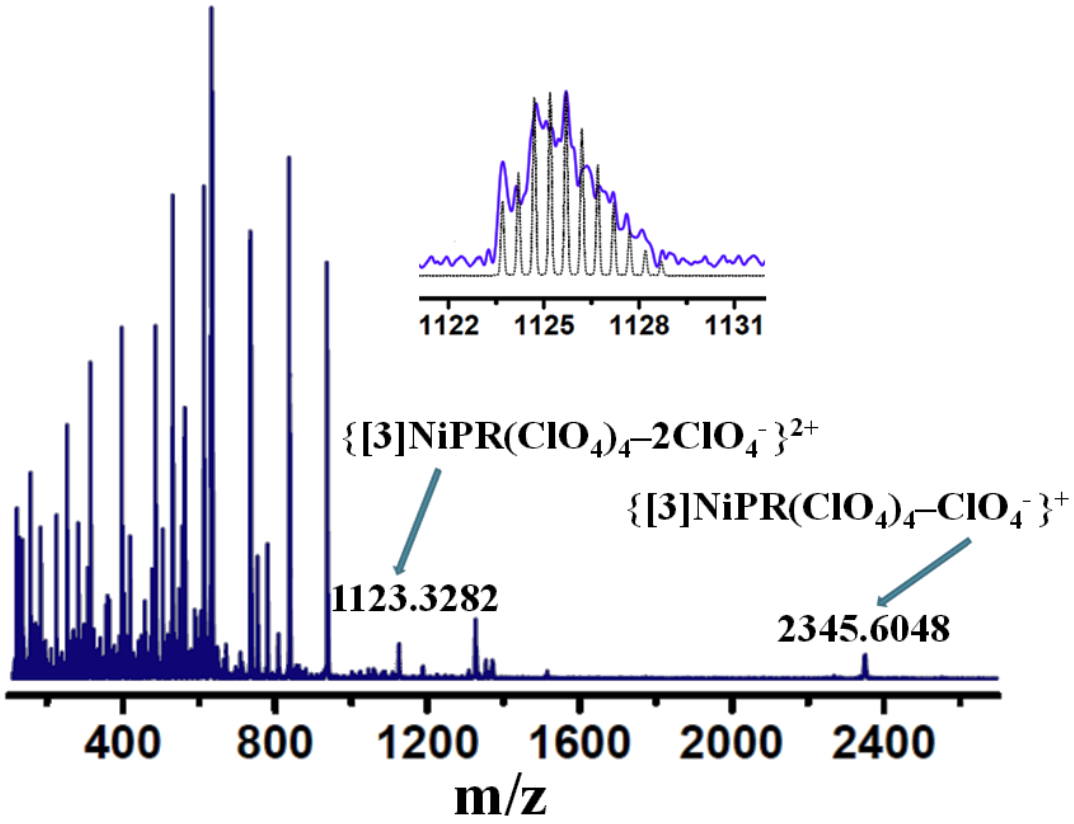

Figure 44S. ESI-MS(+ve) spectrum of **[3]NiPR(ClO$_4$)$_4$** at 298K.

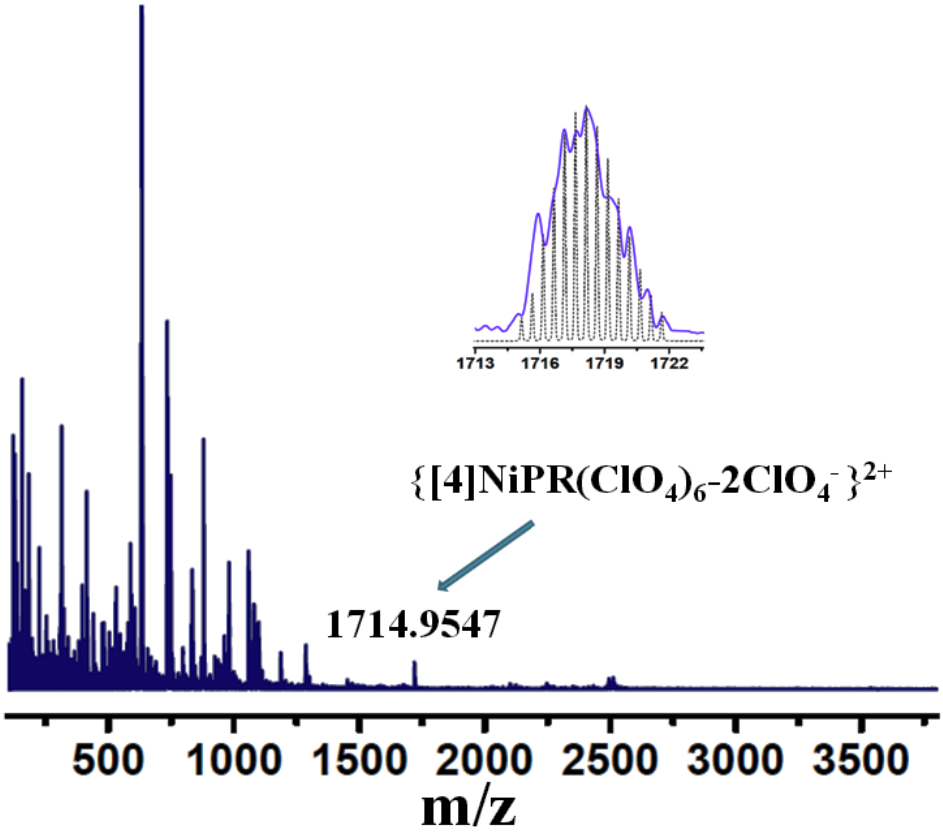

Figure 45S. ESI-MS(+ve) spectrum of **[4]NiPR(ClO$_4$)$_6$** at 298K.

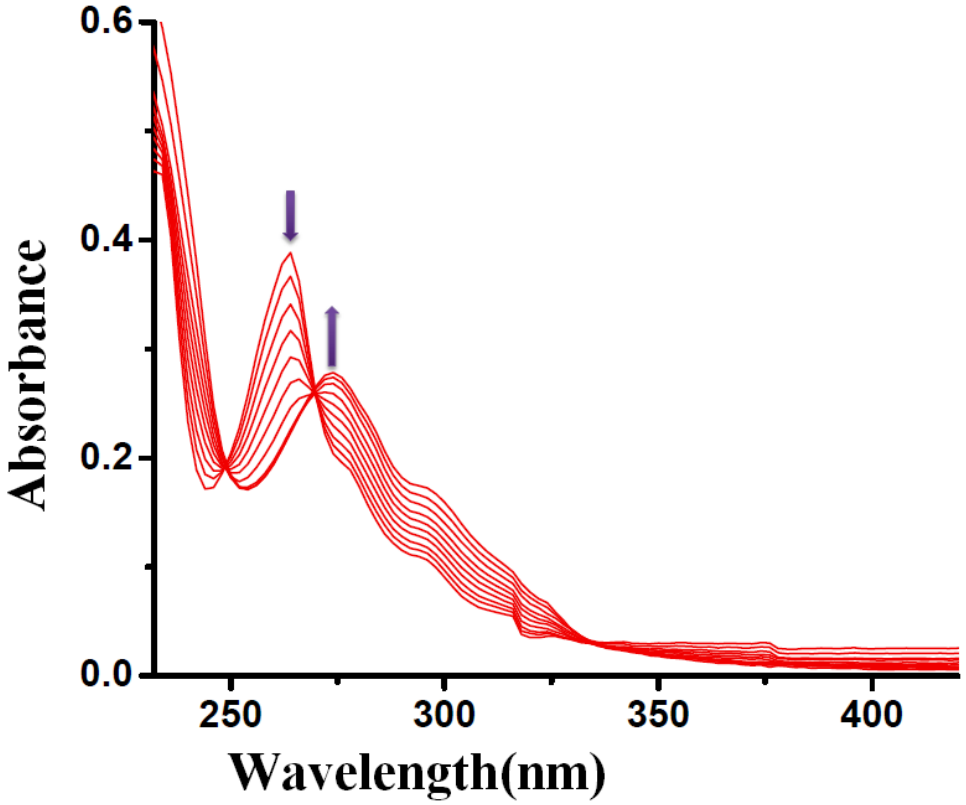

Figure 46S. UV/Vis titration profile between **L1** ($1x10^{-5}$ M) with **NaphMC-Ni**(II) ($1x10^{-4}$ M) in CH_3CN at 298 K.

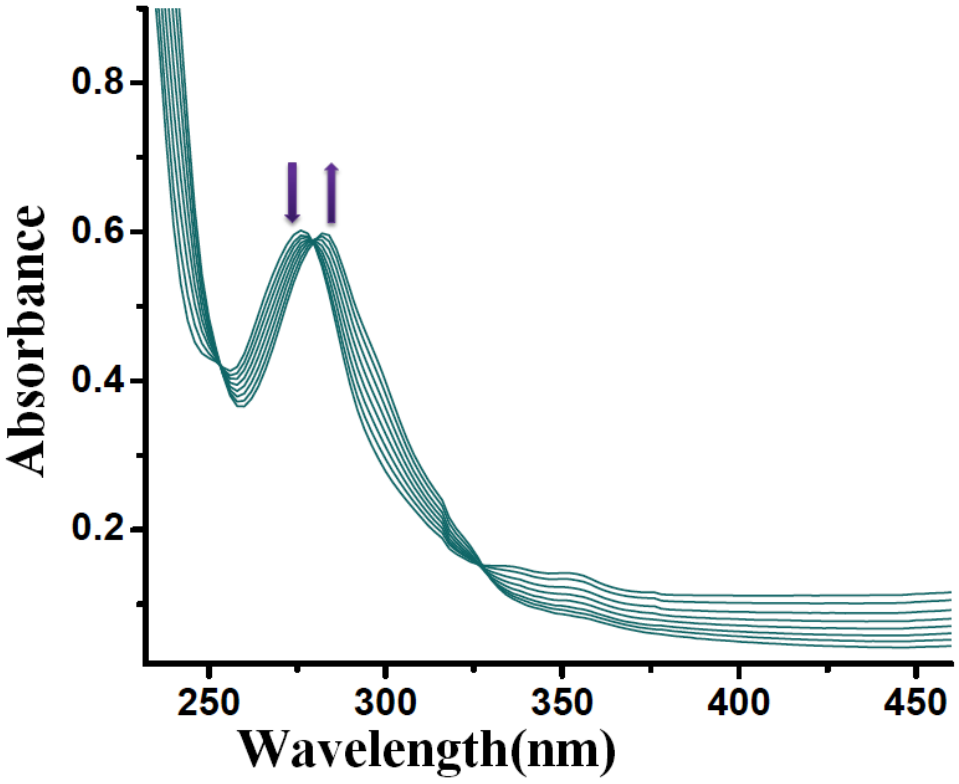

Figure 47S. UV/Vis titration profile between **L2** ($1x10^{-5}$ M) with **NaphMC-Ni**(II) ($2.2x10^{-4}$ M) in CH_3CN at 298 K.

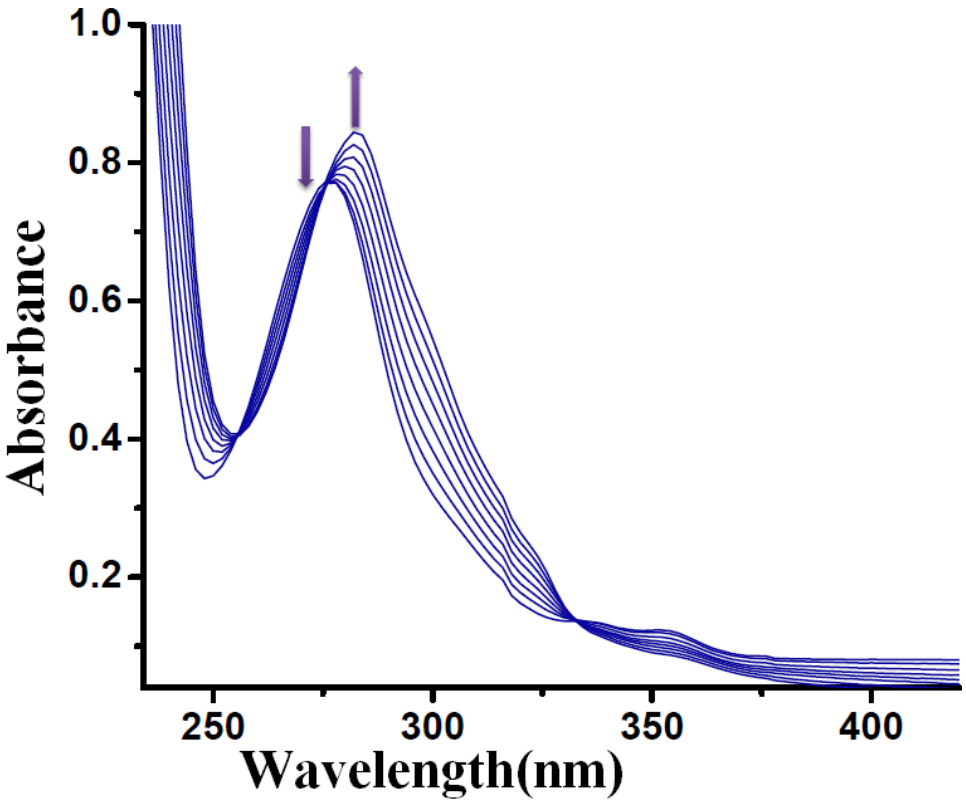

Figure 48S. UV/Vis titration profile between **L3** ($1x10^{-5}$ M) with **NaphMC-Ni**(II) ($3.8x10^{-4}$ M) in CH_3CN at 298 K.

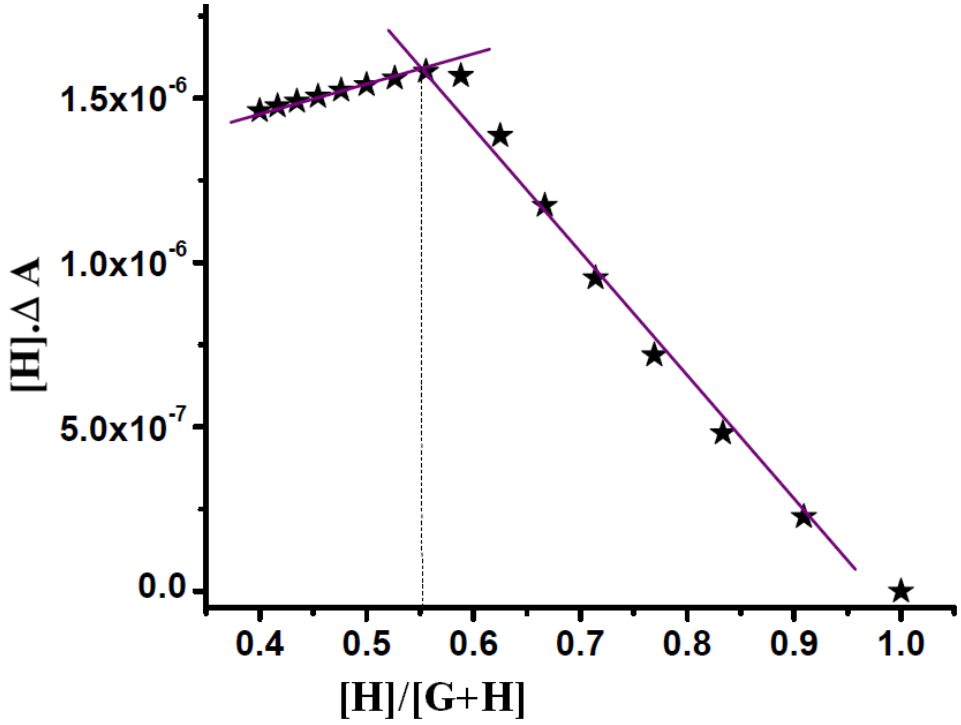

Figure 49S. Molar ratio plot from UV/Vis titration experiment between **Ll** with **NaphMC-Ni(II)** solution.

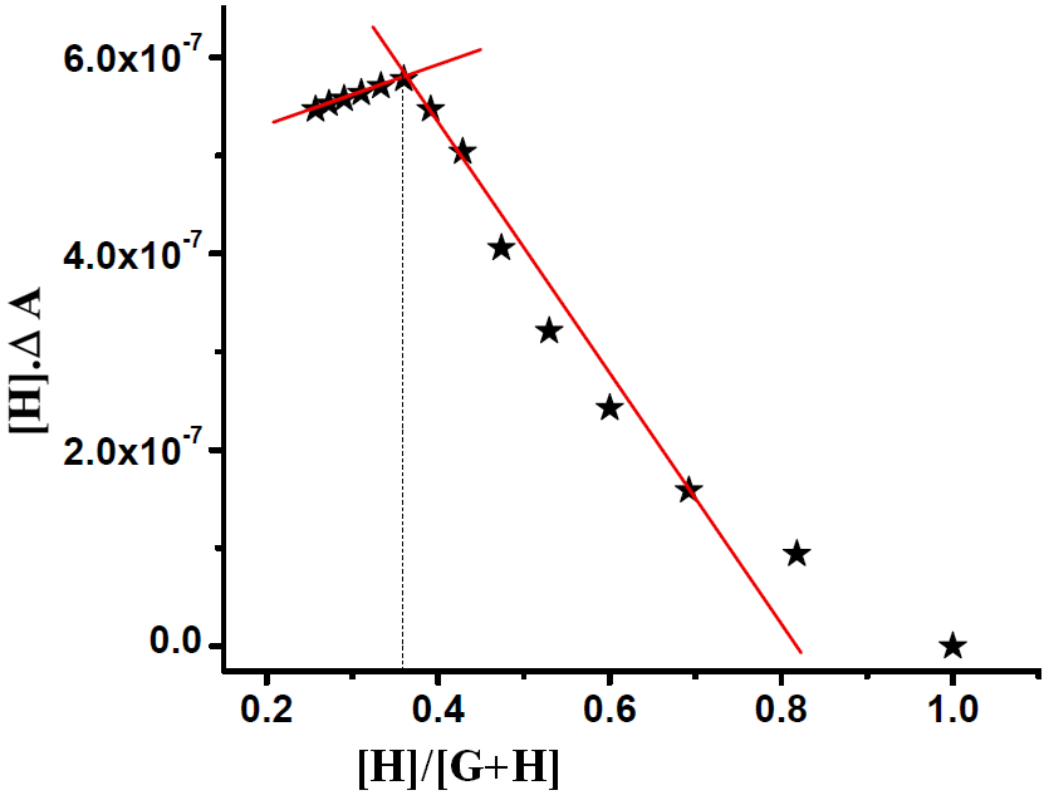

Figure 50S. Molar ratio plot from UV/Vis titration experiment between **L2** with **NaphMC-Ni(II)** solution.

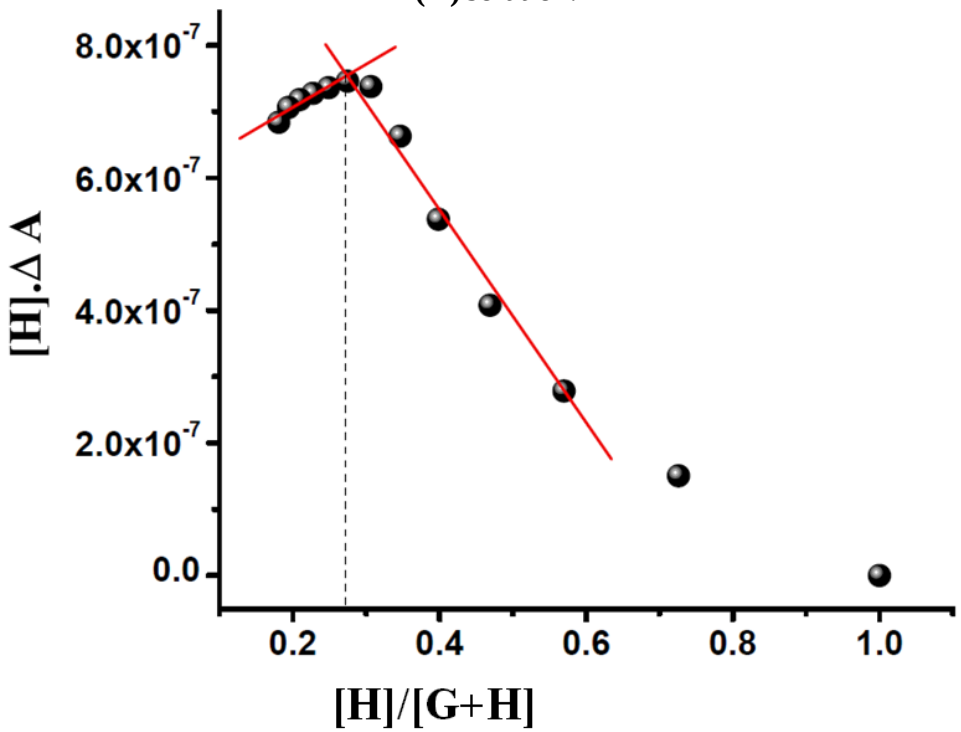

Figure 51S. Molar ratio plot from UV/Vis titration experiment between **L3** with **NaphMC-Ni(II)** solution.

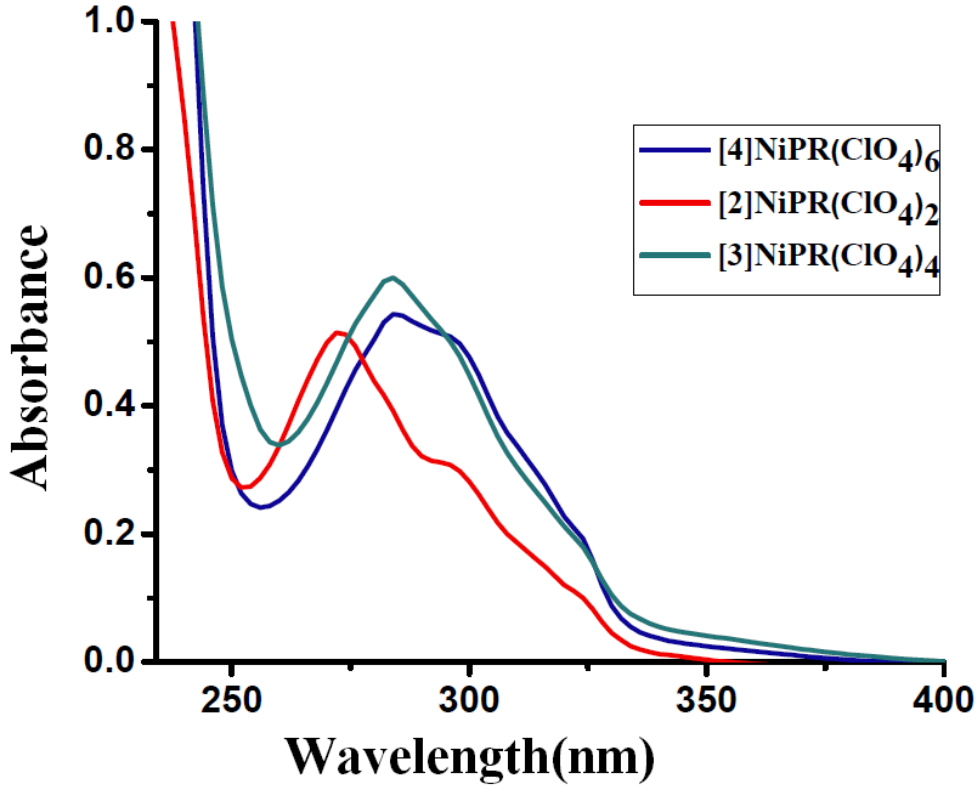

Figure 52S. Characteristic UV/Vis spectra of pseudorotaxanes: **[2]NiPR(ClO$_4$)$_2$**, **[3]NiPR(ClO$_4$)$_4$** and **[4]NiPR(ClO$_4$)$_6$** at 298K.

References

1. APEX2 suite for crystallographic software, Bruker axs, Madison, WI (2009).

2. SAINT - Software for the Integration of CCD Detector System Bruker Analytical X-ray Systems, Bruker axs, Madison, WI (1995).

3. G. M. Sheldrick, SHELXT 14. Program for Crystal Structure Solution and Refinement, University of Göttingen, Göttingen, 2014.

4. O.V. Dolomanov and L.J. Bourhis and R.J. Gildea and J.A.K. Howard and H. Puschmann, Olex2: A complete structure solution, refinement and analysis program, *J. Appl. Cryst.*, (2009), **42**, 339-341.

5. Sheldrick, G.M., Crystal structure refinement with ShelXL, *Acta Cryst.*, (2015), **C71**, 3-8.

6. G. M. Sheldrick, SADABS, Empirical Absorption Correction Program, University of Göttingen, Göttingen, Germany,1997.

7. A. L. Spek, PLATON-97, University of Utrecht, Utrecht, the Netherlands, 1997.

8. Mercury, version 3.7, supplied with Cambridge Structural Database, CCDC, Cambridge, U.K., 2003–2004.

9. (a) J. Cai, B. P. Hay, N. J. Young, X. Yang and J. L. Sessler, *Chem. Sci.*, 2013, **4**, 1560–1567; (b) P. Thordarson, *Chem. Soc. Rev.*, 2011, **40**, 1305–1323.

10. E. Pershagen, J. Nordholm and K. E. Borbas, *J. Am. Chem. Soc.*, 2012, **134**, 9832-9835.

11. S. Bej and P. Ghosh, *Dalton Trans.*, 2018, **47**, 13408-13418.

12. K. Hara, H. Sugihara, L. P. Singh, A. Islam, R. Katoh, M. Yanagida, K. Sayama, S. Murata and H. Arakawa, *J. Photochem. Photobiol., A*, 2001, **145**, 117-122.